ELECTRON TUNNELING STUDIES OF Mn_{12}-ACETATE

A Dissertation

by

LIANXI MA

Submitted to the Office of Graduate Studies of
Texas A&M University
in partial fulfillment of the requirements for the degree of

DOCTOR OF PHILOSOPHY

May 2008

Major Subject: Physics

ELECTRON TUNNELING STUDIES

OF Mn_{12}-ACETATE

A Dissertation

by

LIANXI MA

Submitted to the Office of Graduate Studies of
Texas A&M University
in partial fulfillment of the requirements for the degree of

DOCTOR OF PHILOSOPHY

Approved by:

Chair of Committee,	Glenn Agnolet
Committee Members,	Joseph H. Ross, Jr.
	Jairo Sinova
	Xinghang Zhang
Head of Department,	Edward Fry

May 2008

Major Subject: Physics

ABSTRACT

Electron Tunneling Studies Of Mn_{12}-Acetate. (May 2008)

Lianxi Ma, B.S., Hebei University. P.R. China;

M.S., Hebei University. P.R. China;

Ph.D., Institute of Physics, Chinese Academy of Sciences. P.R. China

Chair of Advisory Committee: Dr. Glenn Agnolet

We used self-assembling tunnel junctions (SATJs) to study the electron transport through films of the molecular magnets, Mn_{12}-Acetate. Pulse laser deposition (PLD) was used to deposit two monolayers of Mn_{12}-Acetate on thin Pt wires (diameter 0.001 in). The electron tunneling current was measured with typical bias voltages from -1 to 1 V at liquid helium temperature, 4.2 K. I, dI/dV, and d^2I/dV^2 signals were directly acquired with the aid of a current amplifier and two lock-in-amplifiers. Results show that the differential conductance is approximately 10^{-6} S for bias voltages 0.04 V $\leq \mid V \mid \leq$ 1 V and exhibits a strong voltage dependence. In the region $\mid V \mid \leq$ 0.04 V, we find a zero-bias feature (ZBF) in which the differential conductance is suppressed. In some samples, we observe $I - V$ staircases which we attribute to electrons "hopping" between the electrodes and the molecules. The observed hysteresis was attributed to the slow relaxation of molecules re-orienting within the junction. Abrupt conductance jumps at a bias voltage of -0.12 V were also observed and may indicate state transitions in the Mn_{12}-Acetate molecules. Furthermore, we observed that the zero bias feature (ZBF) can switch from an enhancement to a suppression of the differential conductance.

A dip and dry (DAD) method was also used to form films of Mn_{12}-Acetate on Al and Pt wires. Although the conductances were similar to those obtained using the

PLD method, there were some subtle differences. In particular, we did not observe the $I - V$ staircases and the state jumps were more ambiguous. The differential conductance for the Mn_{12}-Acetate films on Al wires were typically 10^{-7} S, which we attributed to the oxide layer on Al surfaces.

We have also found substantial changes in the $I - V$ characteristics when the Pt wires coated with the Mn_{12}-Acetate films were stored in 10^{-2} Torr for 6 months. In particular, we observed many new features such as peaks in the conductance as a function as the bias voltage. We believe that these effects may be caused by the slow oxidation of the Mn_{12}-Acetate molecules.

ACKNOWLEDGMENTS

In the Spring of 2003, I asked Dr. Agnolet if he would be my advisor and he said yes. From then on, he has been my advisor and good friend. I made a smart choice. Many times I was impressed by his solid experimental and theoretical knowledge of physics and his positive working attitude and creativity. Furthermore, he impressed me with the attitude that he was always willing to help me in every aspect of my research. If I have questions on academics, I would go to him; if I have problems in my daily life, I would go to him too. In both cases I know that he will do his best to help me and the problems will be most likely solved. More than once, he came down to the laboratory at midnight or during a weekend at my request to help me solve experimental troubles. And after each such time, I would be more impressed by his knowledge. He sets a good example of being a respectable and qualified advisor.

I would like to thank four coworkers in our laboratory: Chen Chi, Chen Xin, Chang Yong and Marcus L. Teague. They were extremely helpful when the experiments ran 24 hours a day for 14 consecutive days. Marcus was very helpful for my learning how to prepare and run the experiment when I came to the laboratory. Chen Chi and Chang Young often helped me run the experiment without saying even once that they were too busy to help me. Dr. Chen Xin was a problem solver to whom I would go when I had any puzzles. I enjoyed the friendly atmosphere in the laboratory and have benefited from their knowledge and suggestions.

My thanks also go to Brad Malone, our student worker who helped me assemble an electrical circuit for a single molecule tunneling experiment.

I need to thank Dr. V. Meenakshi in Dr. Teizer's group for helping me with the PLD technique and for teaching me how to deposit Mn_{12}-Acetate on platinum wires. Thanks also go to D.M. Seo in Dr. Teizer's group for helping me with the DAD

technique and for teaching me how to deposit Mn_{12}-Acetate and C60 on platinum and aluminum wires. Thanks also go to Daya Rathnayaka for his help with the metal evaporation chamber needed to deposit iron on platinum wires. I am grateful to the help from Dr. Liang Gang in Material Characterization Facility in making the AFM and STM pictures of Mn_{12}-Acetate molecules.

I owe special gratitude to my family for their continuous and unconditional support: To my parents for instilling in me confidence and a drive for pursuing my Ph.D. and to my wife, Yufen Fu, my daughter, Lin Ma, for their enduring patience, understanding, and love.

TABLE OF CONTENTS

Page

LIST OF FIGURES

FIGURE Page

FIGURE Page

FIGURE Page

LIST OF TABLES

CHAPTER I

INTRODUCTION

Speculations about the microscopic structure of matter have intrigued human kind for thousands of years. Ancient Greek philosophers, including Leucippus and Democritus, considered the question of what would happen if someone took a small object, like a block of copper, and cut it in half, then cut it in half again, and again, for many subsequent divisions [1]. They reasoned that eventually one would reduce the block to a single speck of copper that could not be divided further. This smallest piece of an element was called the atom (a + tom), which literally means "without division". It was not until the late nineteenth century, however, that the question of atoms began to yield to direct scientific investigation.

In 1897, the English physicist J.J. Thomson discovered a "particle" that was much smaller in size and thousands of times less massive than even the smallest atom [2]. The electron, as this particle was named, was also found to have a negative electrical charge. These microscopic particles exhibited behavior different from large or classical objects. People began to understand these new properties with the development of quantum mechanics that was initiated by the German physicist Max Planck during the years of 1900 and 1901 [3]. Electrons and quantum effects will play an important role in our electron tunneling study.

Let us consider a particle encountering a potential barrier in which the potential energy is larger than the kinetic energy of the particle. From the viewpoint of classical mechanics, this particle would be reflected back - it could never reach the other side of the barrier. In quantum mechanics, however, a particle is described by a

---

The journal style is Physical Review B.

wavefunction Ψ. The probability density to find the particle is $\Psi^*\Psi$, which shows smooth behavior even when the potential energy is discontinuous. When a particle encounters a potential barrier that is higher than its kinetic energy, Ψ does not vanish at the boundary but penetrates into the barrier; decreasing exponentially. For tunnel barriers that are sufficiently thin, there will be a probability that the particle can be found on the opposite side of the potential barrier. In the case that these particles are electrons, the transmission through the barrier produces a tunneling current that can easily be measured.

The first phenomena to be identified and convincingly explained in terms of this tunneling phenomenon were identified in 1928: the alpha decay of some heavy nuclei [4]; ionization of hydrogen atoms in a strong electric field [5]; and electron emission from a cold, clean metal surface in a strong electric field [6]. A significant application of this tunneling phenomenon in scientific research and industry occurred between 1965 and 1971, when Russel D. Young, of the National Bureau of Standards, combined the detection of the tunneling current with a scanning device in order to obtain information about the nature of metallic surfaces [7]. The instrument, named topografiner, altered the separation (z) between the tip and the surface so that, at constant voltage, the tunneling current (or, at constant current, the tunneling voltage) remained constant as the tip was scanned over the surface. By recording the x, y, and z coordinates of the tip, a topographic map of the surface could be obtained. This same principle was later used in the scanning tunneling microscope (STM). The remaining barrier to the development of the STM - more adequate vibration isolation, was achieved through the work of Gerd Binnig and Heinrich Rohrer, at the IBM Research Laboratory in Zurich, Switzerland [8]. In 1986 they shared in the Nobel Prize in Physics for their demonstration of atomic resolution using the scanning tunneling microscope.

Measurement of the dependence of the tunneling current (I) on the bias voltage (V) can also provide information about the properties of the tunnel barrier. In 1966, R.C. Jaklevic and J. Lambe [9] found that when the tunneling electrons interact with molecules located at the metal - oxide interface, it was possible to excite the vibrational modes of the molecules. This interaction causes a step increase in the differential conductance, G, at a bias voltage corresponding to the vibrational frequency ν of the vibrational mode of the molecule, i.e., $eV = h\nu$. In addition dG/dV (or d^2I/dV^2) will exhibit a peak at this voltage that corresponds to the resonance of the particular vibrational mode of the molecule. This principle forms the basis for inelastic electron tunneling spectroscopy (IETS). In a metal-insulator-metal junction (MIM), the first electrode is formed by vapor depositing a metallic film (aluminum) on the surface of a glass or other inert substrate. After growing an oxide layer on the surface of the first electrode, the molecules to be studied are introduced and another metal film (typically lead) is deposited over the oxide layer to form the second electrode. Data is typically taken at low temperatures in order to reduce the noise associated with thermal excitations.

Although IETS has proven useful, it is not without inherent difficulties and systematic problems [10]. In the traditional MIM junction, the oxide layer and the metal film that is deposited directly on top of the molecules can perturb the molecules and cause changes in the spectra of the molecules [11]. Another technical problem is that these junctions must be fabricated and doped with the molecules at room temperature. Furthermore, it is difficult to easily dope junctions with aromatics such as benzene, since they evaporate easily at room temperature [12]. Great care must also be taken in the cleanliness and overall preparation of these thin film junctions to avoid conducting "pinholes" and other contaminants that can cause an electrical short in the junction. If one could fabricate and dope the tunnel junction "in situ"

at low temperatures, then one could easily take the junction apart and reform it if the properties of the junction were unsuitable. Such a device would clearly be a significant improvement.

In 1990, S. Gregory [13, 14] invented the self-assembling tunnel junction (SATJ). A schematic view of the tunneling geometry is shown in Fig. 1. The junction consists of a straight metal wire and a curved wire that are placed in a magnetic field that is parallel to the straight wire. A deflection current is applied to the curved wire and the Ampere magnetic force bends it towards the straight wire. To prevent the wires from making direct contact, a thin gas film is adsorbed onto the wires. A junction is then formed at the contact point between the two wires. Gregory used hydrogen and helium but Zimmerman [10] found that the properties of neon make it an excellent choice for the junction barrier. If the barrier film is sufficiently thin (a few to tens of Angstroms), a measurable tunneling current appears when a voltage is applied between the straight and curved wires. Gregory reported observing a peak in the d^2I/dV^2 as a function of the bias voltage suggesting that IETS could be done using SATJs. Zimmerman and Agnolet [15, 16] were able to confirm this conjecture by introducing C_2H_2 into an SATJ and observing all of the vibrational modes of the molecule.

A. Materials Background

1. Mn_{12}-Acetate

The discovery that individual molecules can function as magnets provided a new approach to the development of nanoscale magnetic materials [17]-[19]. These single molecular magnets (SMMs) [20] have a single-domain magnetic core that, below its blocking temperature, T_B, exhibits the classical macroscopic property of a magnet,

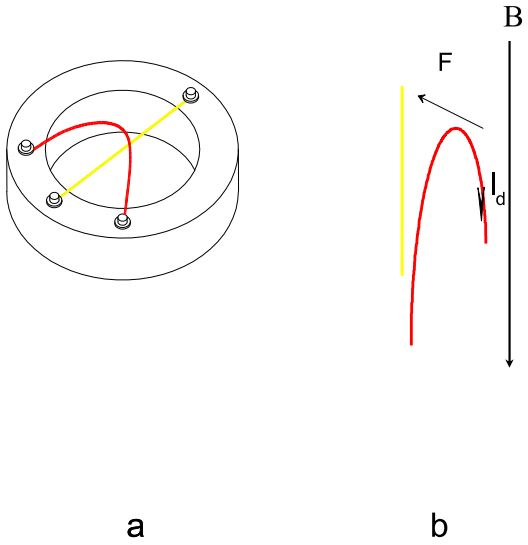

Fig. 1. Schematic view of SATJ. (a) The SATJ consists of a curved wire (red) and a straight wire (yellow) in a magnetic field. (b) When a deflection current I_d is applied to the curved wire, the Ampere force, F, moves the wire towards the straight wire and a junction is formed at the contact point between the two wires. Typically, I_d is 30 mA and the magnetic field is 0.4 T. (Courtesy of Dr. Darin T. Zimmerman in the Department of Physics, Pennsylvania State University, Altoona.)

namely magnetization hysteresis.

Because SMM's exhibit large, bi-stable spin anisotropy and macroscopic quantum behavior [19], they may be useful as magnetic storage devices [21] or as the building blocks for quantum computers. Consequently, they have been extensively studied for the past decade [22]-[29]. After the synthesis of Mn_{12}-Acetate (Mn_{12}-Ac) $[Mn_{12}O_{12}(CH_3COO)_{16}(H_2O)_4]$-2($CH_3COOH$)-4($H_2O$)] (structure is shown in Fig. 2) by T. Lis in 1980 [30], it has become the prototype SMM. As can be seen in Fig. 2, Mn_{12}-Ac consists of a central $Mn(IV)_4O_4$ cube surrounded by a ring of 8 Mn(III) units connected through bridging oxo ligands. Four Mn^{4+} ($3d^3$, S = 3/2) ions are

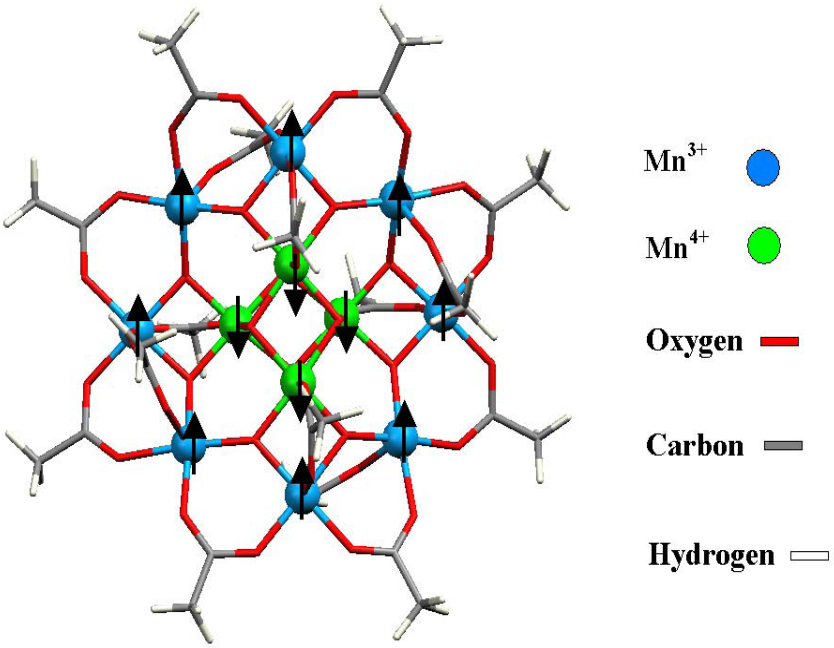

Fig. 2. Schematic view of Mn_{12}-Ac. Four Mn^{4+} ions (green) are ferromagnetically coupled to give a spin $S = 6$; whereas eight Mn^{3+} ions (blue) are ferromagnetically coupled to give a spin $S = 16$ in the opposite direction for a total spin $S = 10$. (Courtesy of Dr. Naresh Dalal in the Department of Chemistry and Biochemistry, Florida State University)

ferromagnetically coupled to one another in a cubane structure that gives rise to a total spin $S = 6$. The remaining eight Mn^{3+} ($3d^4$, $S = 2$) are also ferromagnetically coupled to one another in a crown structure for a total spin of $S = 16$. The Mn^{3+} crown is antiferromagnetically coupled to the inner Mn^{4+} cubane structure, yielding a total net spin of $S = 16 - 6 = 10$ for each molecule. This central complex is then surrounded by sixteen acetate and four water ligands that isolate the Mn ions from the environment.

The spin anisotropy manifests itself as an energy barrier that spins must overcome when switching between the individual magnetic states of the molecule. The spin quantum numbers $\pm m_s$ take on the usual $(2S + 1)$ values: $-S$, $-S + 1 \ldots S - 1$,

S. Although in zero magnetic field, the states at $+m_s$ and $-m_s$ are degenerate, the molecule cannot easily switch between these two states because of the barrier between the states (see Fig. 3). This barrier (U) is defined as:

$$U = |D|S^2$$

where S is the dimensionless total spin value and D is the zero-field splitting parameter. Because the barrier inhibits the switching between the degenerate magnetic states, the larger the barrier, the longer the molecule will remains magnetized. For Mn_{12}-Ac, $D = -0.5$ cm^{-1} and therefore for $S = 10$, the overall barrier height is 50 cm^{-1} (or equivalently 60 K) which would correspond to a bias voltage of $V = k_B T/e = 5.2$ mV.

The blocking temperature, T_B, is defined as the temperature below which the relaxation of the magnetization becomes slow compared to the time scale of a particular experimental technique [31]. The T_B for Mn_{12}-Ac is approximately 3 K [24].

Switching between the m_s levels on opposite sides of barrier can only occur via magnetic quantum tunneling (MQT). In direct MQT, the magnetization vector tunnels from a level on one side of the classical energy barrier to a level on the other side. Phonon assisted MQT occurs when the magnetization vector is first excited to a higher energy m_s level by a phonon and then tunnels through the barrier [32]. The first observation of MQT in Mn_{12}-Ac was reported by Bokacheva et al. [28]. Because the origin of MQT is still not fully understood, we hope that our tunneling results can stimulate further theoretical and experimental investigations.

Magnetic storage devices will require the successful production of thin films of the material. Recently films have been made using various techniques and characterized with different devices [33]-[38]. Interestingly, information about the electronic

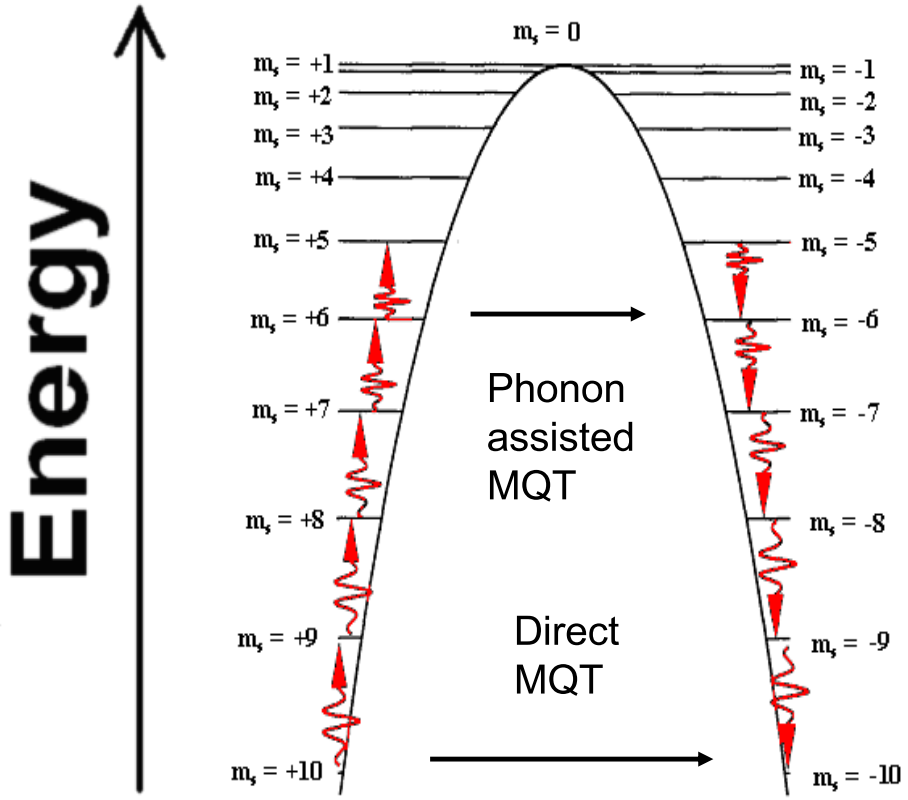

Fig. 3. Schematic view of the energy levels of Mn_{12}-Ac in zero magnetic field. The $\pm m_s$ energy levels are doubly degenerated but are separated by a classical barrier, whose height is given by $\sim |D|S^2$, where D = -0.5 cm^{-1} is the zero-field splitting parameter. (Courtesy of Dr. Naresh Dalal in the Department of Chemistry and Biochemistry, Florida State University)

transport properties are not available for this kind of film although the conductance of the bulk compound was measured from 150 K to 300 K [39]. In reference [39], North et al. reported that the resistance of Mn_{12}-Ac is similar to that of a semiconductor and strongly increases with decreasing temperature. No voltage dependence was reported. At 100 K, the resistance of the Mn_{12}-Ac was too high to be measured with their equipment. By studying the tunneling process in films of Mn_{12}-Ac, we hope to extend these conductance measurements to lower temperatures and study the electron transport in this system.

B. Basic Theory

1. Simple Insulating Barrier

If the insulating film between two electrodes is sufficiently thin, current can flow through the barrier when a voltage is applied between the two electrodes [40]. Sommerfeld and Bethe [41] were the first to make a theoretical study of this phenomena for very low and high voltages. Holm [42] [43] extended this theory to include intermediate voltages. Both studies are based on the WBK (Wentzel-Kramers-Brillouin) approximation.

Sommerfeld and Bethe considered both a rectangular and a symmetric parabolic barrier. J. Simmons [44] determined the tunneling current for a potential barrier of arbitrary shape and, in particular, applied it to a rectangular barrier. In the following, we briefly introduce his derivation.

In the following, we assume that there are no impurity effects, temperature effects, phonon interactions and electron-electron interactions. Consider a thin insulating barrier between two conductors, as shown in Fig. 4. We define the following symbols:

e - charge of the electron;

h - Planck's constant;

η - Fermi energy;

$\phi(x)$ - barrier potential function;

s_1, s_2 - positions at which the potential energy $\phi(x)$ crossed the Fermi level;

$\Delta s = s_2 - s_1$;

J - tunnel current density;

V - voltage across film;

E_x - kinetic energy of the conduction electrons along the x-axis;

ψ - work function of the metal electrodes;

φ_0 - height of the rectangular barrier;

$\overline{\varphi}$ - mean barrier height.

When the barrier potential, $V(x)$, varies slowly with position, the WKB method can be used [45]. For an electron with kinetic energy E_x associated with motion in the x direction, the probability that it penetrates the potential barrier, $D(E_x)$, is given by [44]

$$D(E_x) = \exp\{-\frac{4\pi}{h}\int_{s_1}^{s_2}[2m(V(x) - E_x)]^{1/2}dx\} \tag{1.1}$$

The number of electrons that approach the interface from the left per unit area in a time interval dt is $n(v_x)v_x dv_x dt$, where $n(v_x)$ is the number of electrons per unit volume that have a velocity in the x direction between v_x and $v_x + dv_x$ in the metal. The number of these electrons transmitted through the barrier becomes $n(v_x)D(E_x)v_x dv_x dt$. The total flux of electrons penetrating the barrier is therefore:

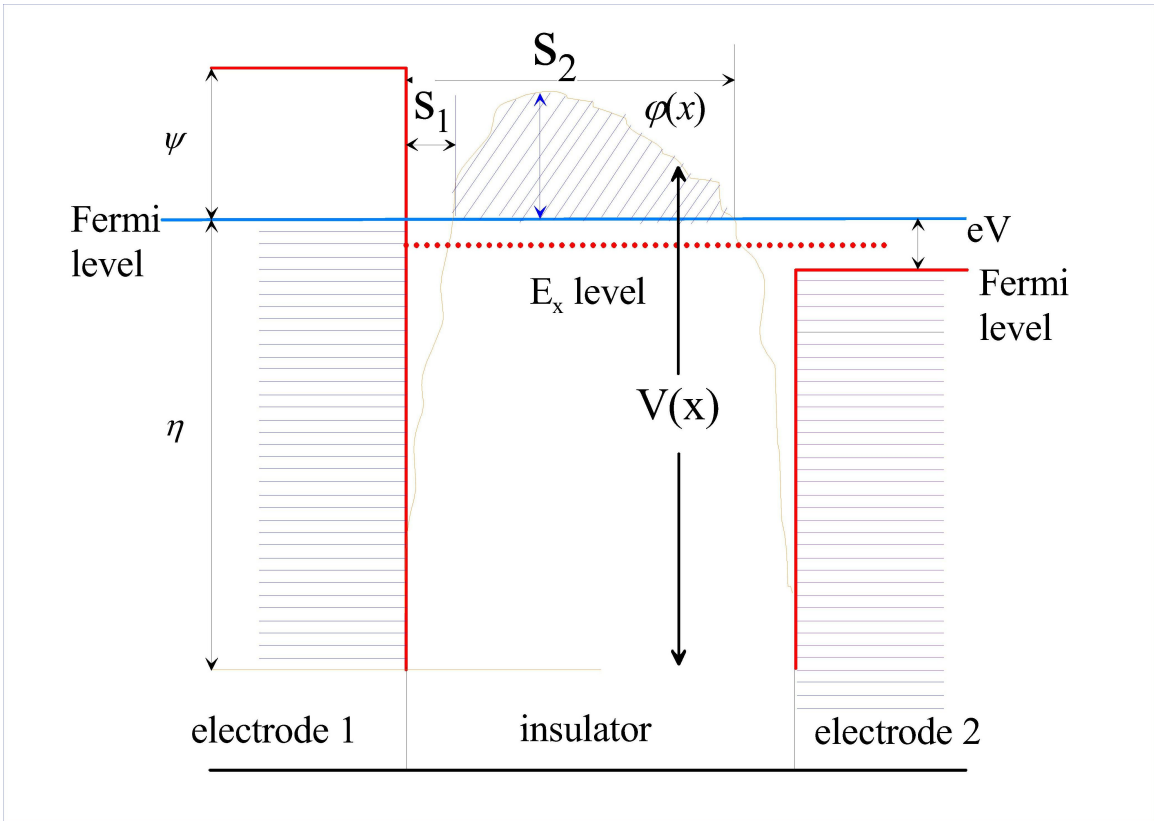

Fig. 4. The potential barrier arising from an insulating film separating two metallic electrodes. The symbols are defined in the text.

$$J_1 = \int_0^{v_m} v_x n(v_x) D(E_x) dv_x = \frac{1}{m} \int_0^{E_m} n(v_x) D(E_x) dE_x \tag{1.2}$$

where v_m and E_m are the maximum velocity and kinetic energy of the electrons respectively. Assuming an isotropic velocity distribution inside the electrodes, the density of electrons with a velocity between v and $v + dv$ is given by:

$$n(v) dv_x dv_y dv_z = \frac{2 dk_x dk_y dk_z}{\left(\frac{2\pi}{L}\right)^3 V} f(E) = \frac{2m^3}{h^3} f(E) dv_x dv_y dv_z \tag{1.3}$$

where $n(v)$ is the number of electrons per volume in $dv_x dv_y dv_z$ and where $f(E)$ is the Fermi – Dirac distribution function, $f(E) = \frac{1}{1+e^{\frac{E-\eta}{kT}}}$,

$$n(v_x) = \frac{2m^3}{h^3} \int \int_{-\infty}^{\infty} f(E) dv_y dv_z = \frac{4\pi m^2}{h^3} \int_0^{\infty} f(E) dE_r \tag{1.4}$$

where we have used the fact that $dv_y dv_z = 2\pi v_r dv_r = 2\pi d(v_r^2/2) = (2\pi/m) dE_r$, and $E_r = (1/2)mv_r^2$ is the transverse kinetic energy. Substituting (1.4) into (1.2) yields

$$J_1 = \frac{4\pi m}{h^3} \int_0^{E_m} D(E_x) dE_x \int_0^{\infty} f(E) dE_r \tag{1.5}$$

Similarly, the flux of electrons tunneling in the opposite direction, J_2, is given by

$$J_2 = \frac{4\pi m}{h^3} \int_0^{E_m} D(E_x) dE_x \int_0^{\infty} f(E + eV) dE_r \tag{1.6}$$

so that the net flux of electrons J becomes

$$J = J_1 - J_2 = \frac{4\pi m}{h^3} \int_0^{E_m} D(E_x) dE_x \left\{ \int_0^{\infty} \left(f(E) - f(E + eV) \right) dE_r \right\} \tag{1.7}$$

Substituting

$$\xi_1 = \frac{4\pi me}{h^3} \int_0^{\infty} f(E) dE_r$$

$$\xi_2 = \frac{4\pi me}{h^3} \int_0^{\infty} f(E + eV) dE_r$$

and

$$\xi = \xi_1 - \xi_2$$

the resultant current density becomes

$$J = \int_0^{E_m} D(E_x) \xi dE_x \tag{1.8}$$

Setting $V(\mathrm{x})=\eta+\varphi(x)$, (Note that $V(x)$ is simply the barrier height rather than the bias voltage), then,

$$D(E_x) = \exp\left\{-\frac{4\pi}{h}\int_{s_1}^{s_2}\left[2m(\eta+\varphi(x)-E_x)\right]^{\frac{1}{2}}dx\right\} \tag{1.9}$$

Replacing $\varphi(x)$ with its average and assuming the barrier is sufficiently thin, then using Eq. (A.5), one obtains

$$D(E_x) \approx \exp[-b(\eta+\overline{\varphi}(x)-E_x)]^{\frac{1}{2}} \tag{1.10}$$

where

$$\overline{\varphi} = \frac{1}{\Delta s}\int_{s_1}^{s_2}\varphi(x)dx$$

$b=\sqrt{2m}(4\pi\beta\Delta s/h)$ and $\Delta s = s_2 - s_1$. β is the result of the approximations made in the Appendix and is approximately equal to 1. Substituting the Fermi function

$$f(E) = \frac{1}{1+e^{\frac{E-\eta}{kT}}}$$

we obtain at $T=0$

$$\xi_1 = \left\{\begin{array}{cc} (4\pi me/h^3)(\eta-E_x) & 0<E_x<\eta \\ 0 & E_x>\eta \end{array}\right\}$$

$$\xi_2 = \left\{\begin{array}{cc} (4\pi me/h^3)(\eta-E_x-eV) & E_x<\eta-eV \\ 0 & E_x>\eta-eV \end{array}\right\}$$

$$\xi = \left\{\begin{array}{cc} (4\pi me/h^3)(eV) & 0<E_x<\eta-eV \\ (4\pi me/h^3)(\eta-E_x) & \eta-eV<Ex<\eta \\ 0 & E_x>\eta \end{array}\right\} \tag{1.11}$$

Substituting Eqs. (1.10) and (1.11) into (1.8) gives

$$\begin{aligned} J &= \frac{4\pi me}{h^3}\Bigg\{eV\int_0^{\eta-eV}\exp[-b(\eta+\overline{\varphi}-E_x)^{1/2}]dE_x \\ &\quad + \int_{\eta-eV}^{\eta}(\eta-E_x)\exp[-b(\eta+\overline{\varphi}-E_x)^{1/2}]dE_x\Bigg\} \end{aligned} \tag{1.12}$$

Assuming $b(\overline{\varphi}+eV)^{1/2} >> 1$, this equation can be integrated to obtain

$$J = J_0\left\{\overline{\varphi}\exp(-b\overline{\varphi}^{1/2}) - (\overline{\varphi}+eV)\exp[-b(\overline{\varphi}+eV)^{1/2}]\right\} \tag{1.13}$$

where

$$J_0 = \frac{e}{2\pi h(\beta\Delta s)^2}$$

Note that J_0 depends on the bias voltage through the dependence of Δs. Assuming that the potential barrier is rectangular in shape, the voltage dependence of the conductance can be divided into three distinct regions. (see Fig. 5).

(1) $V \sim 0$:

$$\begin{aligned} J &= J_L\varphi_0^{1/2}V\exp\left(-b\varphi_0^{1/2}\right) \\ J_L &= \left[\sqrt{2m}/s\right]\left(\tfrac{e}{h}\right)^2 \end{aligned} \tag{1.14}$$

where Δs is the entire width of the barrier s.

(2) For intermediate voltages but with $V < \varphi_0/e$,

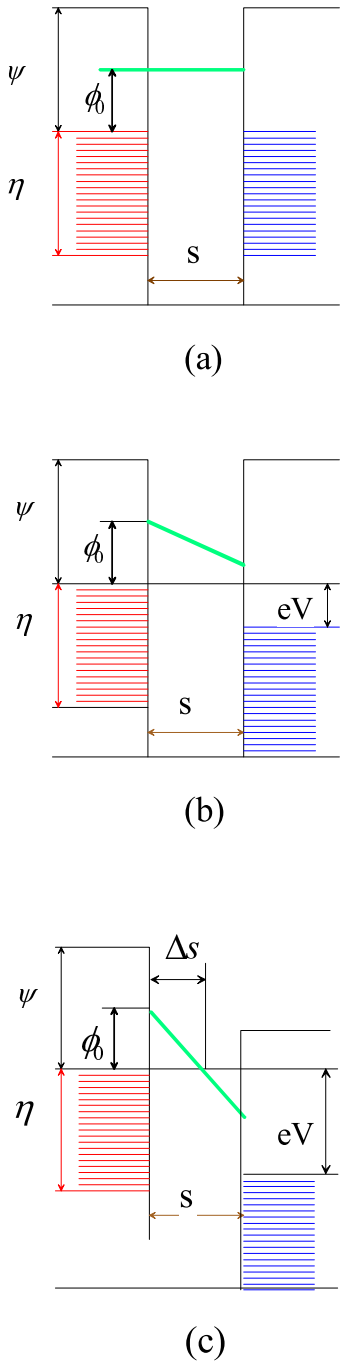

Fig. 5. The rectangular-shaped potential barrier for three different ranges of the bias voltage. (a) The bias voltage is zero and the Fermi levels on both metals are the same. (b) $V < \varphi_0/e$ and the Fermi level on metal 2 is lowered by eV. (3) $V > \varphi_0/e$ and $\Delta s < s$.

$$J = \left(\frac{e}{2\pi h s^2}\right)\left\{\left(\varphi_0 - \frac{eV}{2}\right)\exp\left[-\frac{4\pi s}{h}\sqrt{2m\left(\varphi_0 - \frac{eV}{2}\right)}\right] - \left(\varphi_0 + \frac{eV}{2}\right)\exp\left[-\frac{4\pi s}{h}\sqrt{2m\left(\varphi_0 + \frac{eV}{2}\right)}\right]\right\} \quad (1.15)$$

3) For $V > \varphi_0/e$,

$$J = \left(\frac{2.2e^2F^2}{8\pi h\varphi_0}\right)\left\{\exp\left[-\frac{8\pi}{2.96heF}\sqrt{2m\varphi_0^3}\right] - \left(1 + \frac{2eV}{\varphi_0}\right)\exp\left[-\frac{8\pi}{2.96heF}\sqrt{2m\varphi_0^3(1 + \frac{2eV}{\varphi_0})}\right]\right\} \quad (1.16)$$

where $\overline{\varphi} = \varphi_0/2$ and $F{=}V/s$. For a detailed derivation, see Ref. [44].

In our experiment, we have found that high bias voltages will damage the junction. Therefore, we normally operate with bias voltages less than 2 V which corresponds to the first two regions.

When $eV \ll \varphi_0$, Eq. (1.15) can be expanded in a Taylor power series with respect to V. To third order,

$$J = a\varphi_0\exp\left(-b\varphi_0^{1/2}\right)\left\{\left(-2 + b\varphi_0^{1/2}\right)\frac{eV}{2\varphi_0} + \frac{b\varphi_0^{1/2}}{24}\left(-3 - 3b\varphi_0^{1/2} + b^2\varphi_0\right)\left(\frac{eV}{2\varphi_0}\right)^3\right\} \quad (1.17)$$

where $a = \frac{e}{2\pi h s^2} = \frac{6.2\times10^{+14}}{s^2}$, $b = \sqrt{2m}(4\pi\beta\Delta s/h) = 1.025s$, where s is expressed in Angstroms. The differential conductance per unit area therefore becomes:

$$
\begin{aligned}
g(V) &= \frac{dJ}{dV} \\
&= \left(\frac{6.2\times10^{+14}}{s^2}\right)\exp\left(-1.025s\varphi^{1/2}\right)\left[\left(-2+1.025s\varphi^{1/2}\right)\right. \\
&+ \left.\frac{3.2\times10^{-2}}{s\varphi^{3/2}}\left(-3-3.075s\varphi^{1/2}+1.051s^2\varphi\right)V^2\right] \qquad (1.18)
\end{aligned}
$$

where φ is expressed in the unit of eV and $g(V)$ has units $\mathrm{AV^{-1}m^{-2}}$. As one can see from Eq. (1.18), $g(V)$ depends quadratically on V.

Brinkman et al. [46] considered the problem in which the work functions for the two electrodes are different, φ_1 (electrode 1) and φ_2 (electrode 2). When φ_1=φ_2, his results agree with our expression for the conductance.

In Fig. 6, we illustrate the dependence of the flux, J, on the bias voltage in the range $-2 < V < 2$ from Eq. (1.15) for different thicknesses, s, and barrier heights, φ. We can see that when s changes from 20 Å to 20.5 Å (Fig. 6a), the current density decreases dramatically and when the barrier height increases from 5 eV to 5.15 eV, the flux also decreases (Fig. 6b). In these examples, the value of φ was chosen to be approximately that of the work function of platinum (5.56 eV). The dependence of dJ/dV and d^2J/dV^2 on the bias voltage as expressed in Eq. (1.15) are shown in Fig. 7 with $s = 20$ Å and $\varphi = 1$ eV.

2. Kondo Resonance

The Kondo effect arises from the quantum mechanical interplay between the electrons of the host metal and a magnetic impurity, which causes changes in the local charge and spin variations around the magnetic impurity [47]. For temperatures below a characteristic Kondo temperature T_K, the interaction between the spin of the Kondo impurity and the spins of the surrounding conduction electrons causes

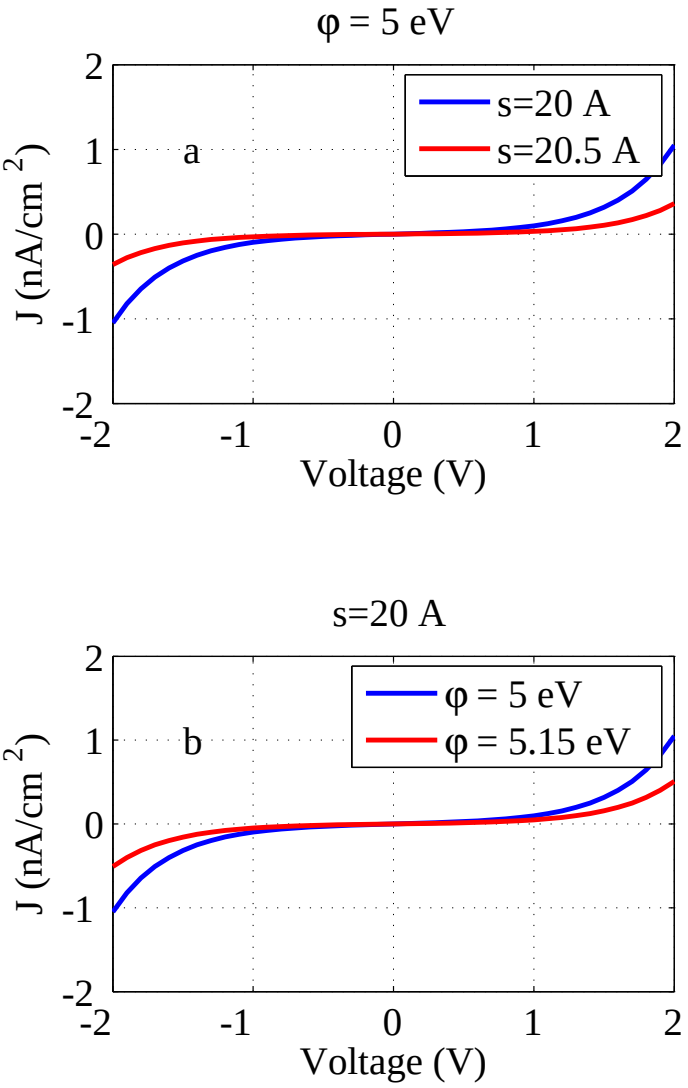

Fig. 6. The voltage dependence of the flux for different insulator film thicknesses, s, and potential barrier heights, φ. It is clear that J strongly depends on s and φ. (a) Dependence on s assuming $\varphi = 5$ eV; (b) Dependence on φ assuming $s = 20$ Å. In both examples, J increases linearly with V at low voltages, but increases more rapidly with increasing V.

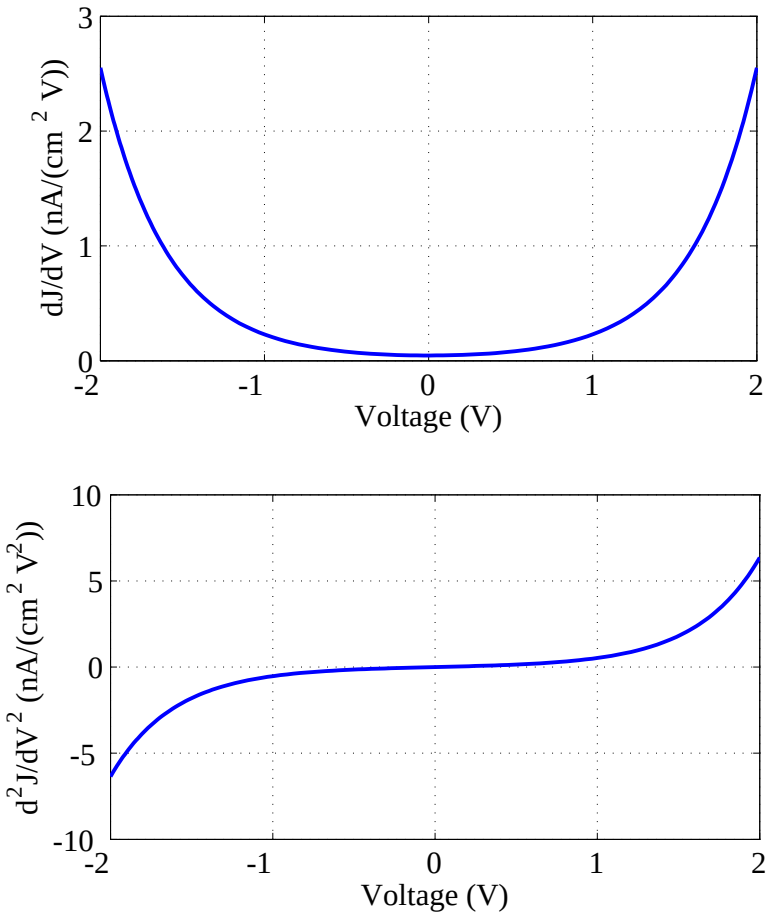

Fig. 7. The voltage dependence of (a) dJ/dV; (b) d^2J/dV^2. Both plots assume $s = 20$ Å and $\varphi = 5$ eV.

the electrons of the host metal to condense into a many-body ground state that collectively screens the local spin of the Kondo impurity [48]. This screening cloud exhibits a dense set of low-energy excitations called the Kondo resonance [49]. V. Madhavan, et al. have observed a Kondo resonance in dI/dV vs. V when the probe of a STM scans over a cobalt (Co) atom on the surface of gold (Au) [50]. To interpret this behavior, one must consider the excitation spectrum that is predicted for a magnetic atom upon the addition or subtraction of an electron.

To understand this behavior it is useful to use the framework of the Anderson model of a magnetic impurity [51]. According to this model, a Co atom on Au can be treated as a discrete d orbital in resonance with the continuum of Au conduction-band states. When the d orbital is occupied by only one electron the energy is ϵ_d, whereas the energy to add a second electron is $\epsilon_d + U$, where U represents the Coulomb interaction between the two electrons in the d orbital ($U = 0$ for the noninteracting case). As might be expected, the d orbital in this model spreads into a relatively broad d resonance that lies below Fermi energy E_F [51]. However, below T_K some of the d-orbital spectral density is shifted to the states at the Fermi surface, forming a narrow, nearly Lorenzian resonance there. This is the many-body Kondo resonance, and the width of the resonance, ΔE, is proportional to the Kondo temperature, $\Delta E \propto k_B T_k$. When tunneling into the Kondo resonance, one might expect dI/dV to reflect this d-orbital spectral density and yield a Lorentzian-like peak about E_F [52]. Such an interpretation, however, assumes that electrons can only tunnel into the orbital of the magnetic impurity and completely ignores the electron tunneling into the surrounding continuum of conduction-band states. An electron tunneling from an STM tip to the Kondo resonance actually has two possible channels (the d orbital and the continuum) and this leads to an additional interference term. We believe that some of the features observed in our SATJ can be explained in terms of the simultaneous tunneling into these two channels.

This problem was systematically studied by Fano [53]. Fano calculated the effect of the interference for transitions from an arbitrary initial state to a noninteracting discrete state in resonance with a continuum (that is, the $U = 0$ case of the Anderson model). He has shown that the rate of transitions to a final state at energy ε can be expressed as

$$R(\varepsilon) = R_0(\varepsilon)\frac{(q+\varepsilon')^2}{1+\varepsilon'^2} \tag{1.19}$$

where

$$\varepsilon' = \frac{\varepsilon - \varepsilon_0}{\Gamma/2},$$

ϵ_0 is the energy of the discrete state, Γ is the width of the resonance, $R_0(\epsilon)$ is the transition rate in the absence of the discrete state, and q is the ratio of the matrix elements linking the initial state to the discrete and continuum parts of the final state. Y. Meir and N. S. Wingreen [54] generalized this expression to include an interacting resonant level (for $U \neq 0$) by changing ϵ' to

$$\varepsilon' = \frac{\varepsilon - \varepsilon_0 - Re\left[\Sigma(\varepsilon)\right]}{Im\left[\Sigma(\varepsilon)\right]} \tag{1.20}$$

Here $\Sigma(\epsilon)$ is the full self-energy of the resonant level including both interactions and coupling to the continuum. Near the Kondo resonance at E_F, the real and imaginary parts of the self-energy can be expressed as [55]

$$Im\left[\Sigma(\varepsilon)\right] = \Gamma/2$$

and

$$\varepsilon - \varepsilon_0 - Re\left[\Sigma(\varepsilon)\right] = \frac{(\varepsilon - \alpha)\,\Gamma}{2k_B T_K}$$

where α is a constant and T_K is the Kondo temperature above which the Kondo effect will disappear. The differential conductance, $\mathrm{d}I/\mathrm{d}V$, of the tunnel junction, is a measure of the rate of electronic transitions from the state at E_F on the negatively biased wire to the states at $E_F + eV$ on the positively biased wire [56] or alternatively the density of electron-like excitations of the positively biased wire at an energy eV measured with respect to E_F. Therefore, one can directly determine the spectrum of

a Kondo resonance by measuring $\mathrm{d}I/\mathrm{d}V$.

In Fig. 8, we illustrate typical results based on on Eq. (1.19). Note that the interference of a discrete autoionized state with a continuum gives rise to characteristically asymmetric peaks in the plot, similar to those observed in our experiment.

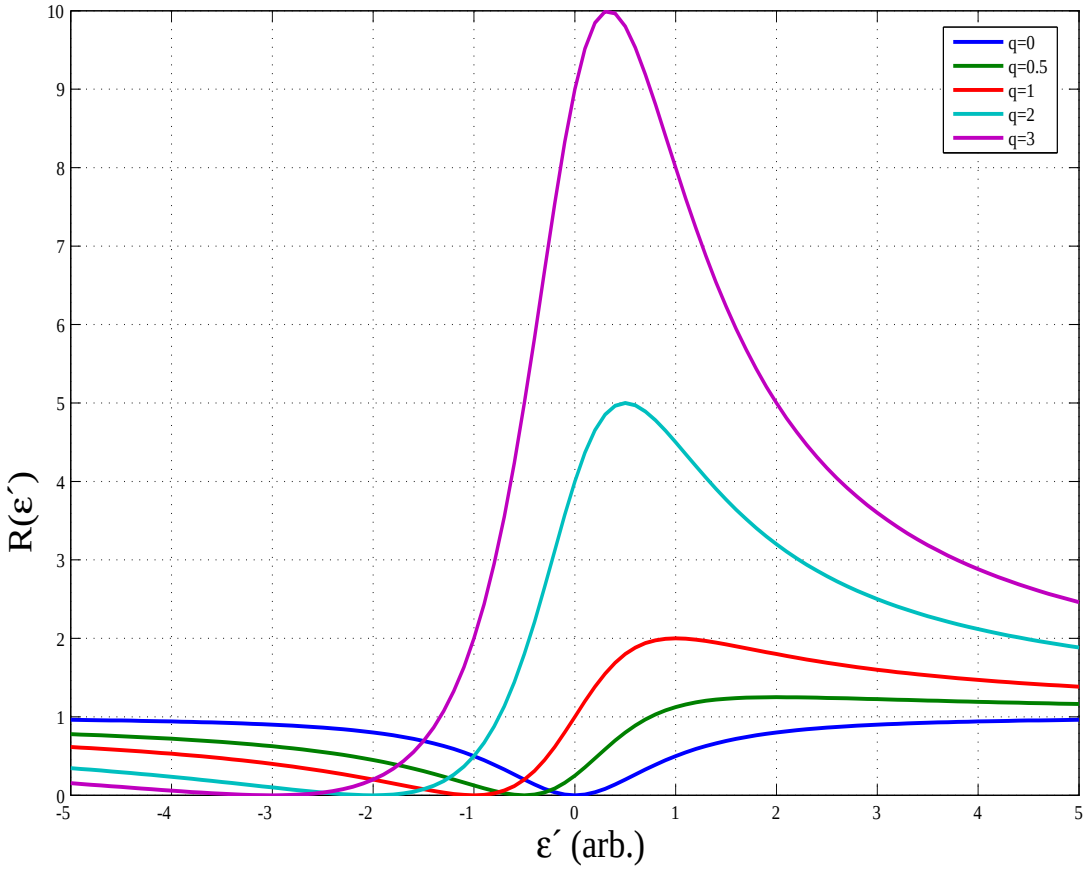

Fig. 8. Transition rate based on Eq. (1.19) assuming $R_0 = 1$. Note that peaks are very asymmetric. q values are indicated in the legend.

CHAPTER II

EXPERIMENTAL APPARATUS AND PROCEDURES

A. Experimental Apparatus

1. Cryostat

The measurements presented here were all made on a compact ^{4}He cryostat (Fig. 9) that can be inserted into a portable helium storage Dewar. Because this cryostat was described in detail in the thesis of Dr. D. T. Zimmerman [10], we will only give a brief introduction. The tunneling wires are mounted on a copper ring that is attached to the bottom of the 1 K pot and the entire experimental section of the cryostat is sealed within a vacuum can. To cool the system, the cryostat is inserted into a custom 100-L liquid helium dewar. Although most of the measurements were made at 4.2 K, temperatures down to 1.5 K can be achieved by pumping on the 1 K pot. For a full dewar of liquid He, the experiment can be continuously operated for 15 days, enabling us to take numerous I-V traces and to check their reproducibility.

The SATJ mount can accommodate three wires, two curved and one straight. In any given measurement, only one straight wire and one curved wire can be used at a time. The extra curved wire gives us the option to switch wires if one of the wires fails and makes it possible to compare the behavior of wires made from or coated with different materials in a given cool-down. (The extra curved wire is not shown in Fig. 1). Each wire is connected in a four-terminal configuration so that the temperature of the wire can be monitored when the surfaces of the wires are cleaned by Ohmic heater. The bias voltage is always applied between the straight and curved wires.

On bare wires, the insulating film is formed by dosing appropriate amounts of neon gas into the cryostat. The melting point and boiling point of neon are 24.56 K

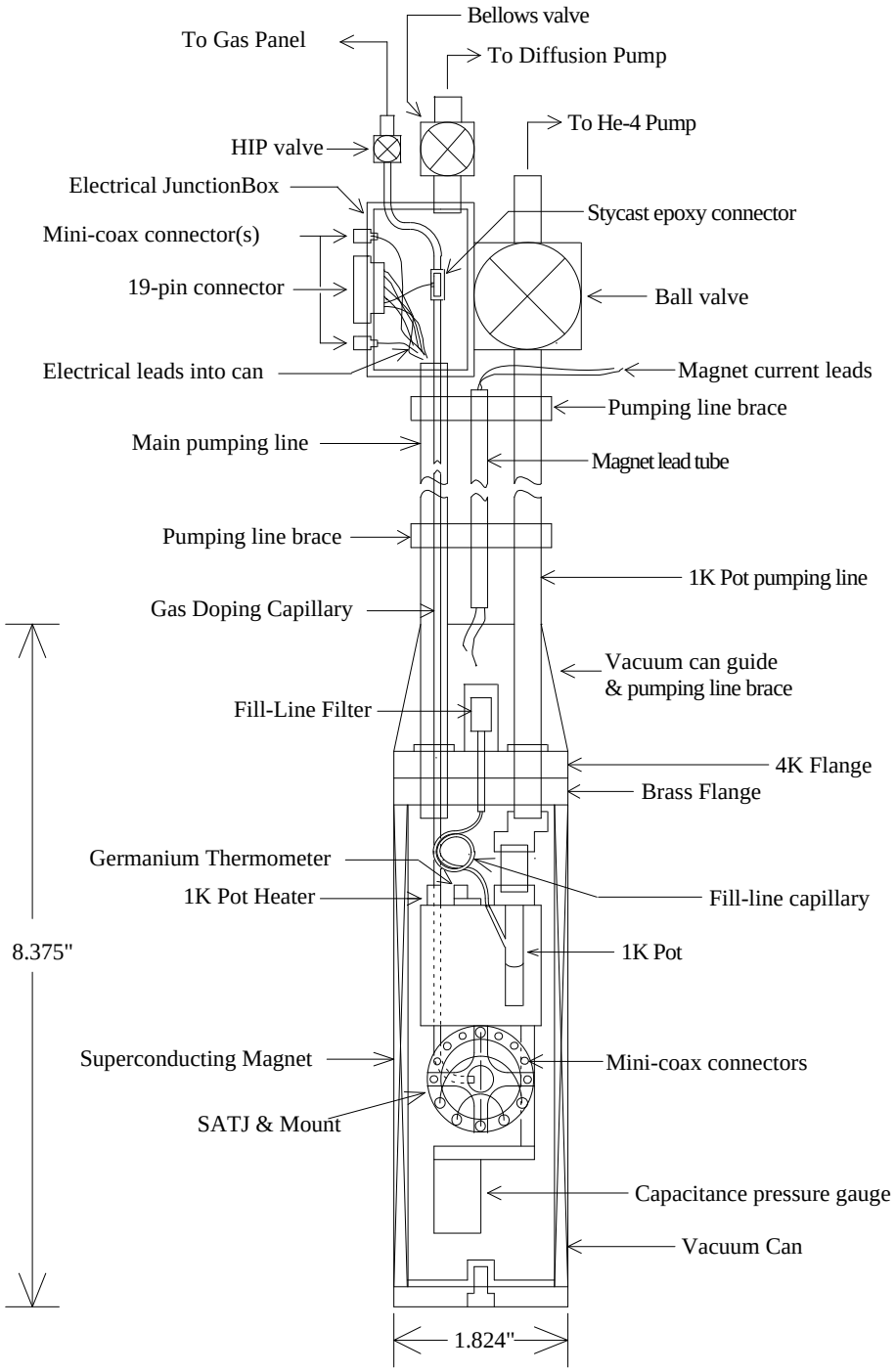

Fig. 9. Detailed view of SATJ cryostat built by D.T. Zimmerman. Specific details can be found in his thesis [10].

and 27.07 K respectively. Zimmerman [10] found that at liquid helium temperatures, the neon is sufficiently soft that the separation between the wires, and therefore the resistance of the junction, can be manipulated by changing the magnetic force on the curved wire. When the wires are coated with Mn_{12}-Ac or C60, no neon layer was required to obtain an insulating barrier but in some measurements, neon was added to improve the stability of the junction.

The ambient magnetic field is provided by a superconductor solenoid wound on the exterior of the vacuum can. When a deflection current is applied to the curved wire, the Ampere force makes the curved wire move toward the straight wire and the tunneling junction is formed at the contact point between the two wires.

In these experiment, we have used platinum, iron, and aluminum wires that are approximately 0.001" in diameter and 1.5 cm in length. These wires are attached to the copper mount using small copper posts that are made from 0.010" diameter bare copper wires. The tunneling wires are first wrapped around the copper posts and then fixed in position with PbSn solder. Although silver print and silver epoxy have also been used to connect the wires to the copper post, this results in a large contact resistance (typically 1 to 10 Ohms) and consequently a large offset in the measurements of the bias voltage.

2. Laser Deposition of the Mn_{12}-Acetate Film

Pulsed laser deposition (PLD) was used to deposit the Mn_{12}-Ac films onto the platinum wires. A sample of Mn_{12}-Ac was obtained from Prof. K. Dunbar's group in the Chemistry Department at TAMU. The PLD system is located in the lab of Prof. D. G. Naugle in the Physics Department and was operated by Dr. V. Meenakshi, a post-doctoral associate working with Prof. W. Teizer also in the Physics Department.

To obtain a more uniform deposition on the wires, the wires were mounted on

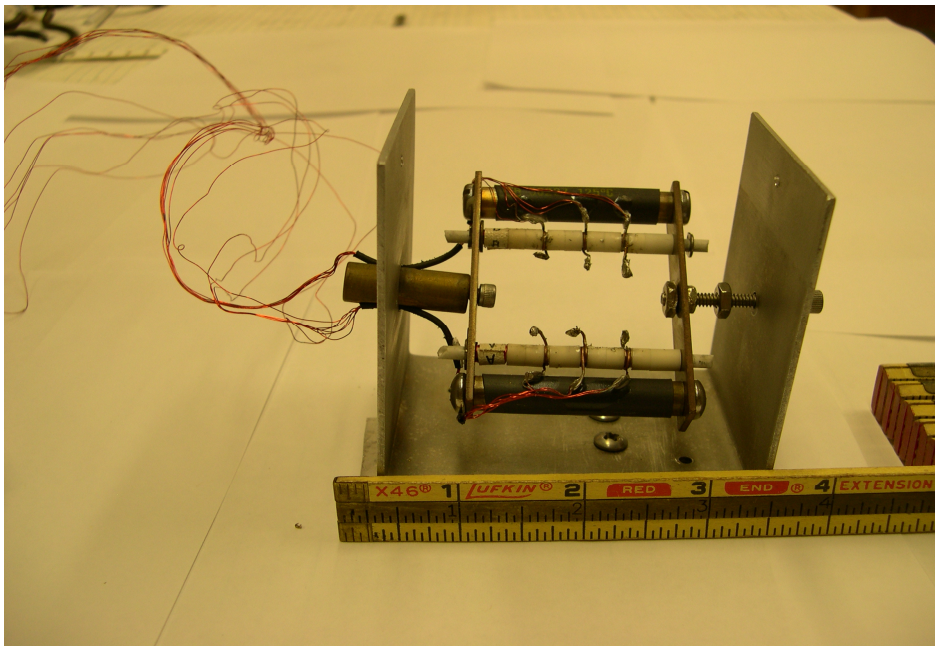

Fig. 10. Frame for rotating the tunneling wires in the PLD chamber during deposition. The two black posts are brass that were wrapped with shrink tubing so that the wires can be attached to them and still be insulated from one another. The two white posts are ceramic. Ceramic rings are also inserted between the conduction wires to prevent them from making contact. A spring (not shown in the picture) is attached at one end (yellow brass) of the frame and connects to the external manipulator of the chamber.

a rectangular frame that can be manually rotated from outside of the deposition chamber (see Fig. 10). By rotating the wire frame between depositions, both surfaces of the wires can be coated with Mn_{12}-Ac films.

Three pairs of electric connectors were attached to two ceramic posts and separated by two ceramic insulation rings. One platinum wire is mounted between each pair of connectors. The voltage and current applied to the wires is monitored using a four-terminal technique. The 12 wires go to a 12-pin connector that connects to the external power supply, ammeter, and voltmeter.

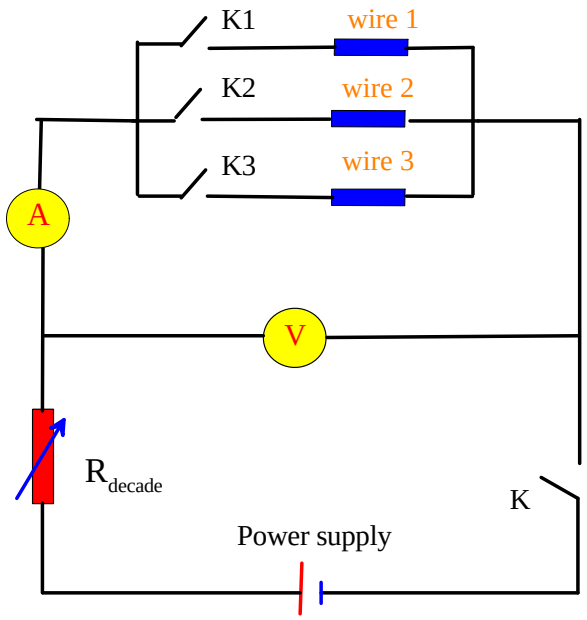

Fig. 11. Circuit used to heat wires in PLD chamber. The current is controlled by an adjustable decade resistor, R_{decade}, in series with the wires and a 10V DC power supply. Each individual wire is heated in turn for approximately 15 minutes.

The electrical circuit is shown in Fig. 11. The platinum wire is approximately 1.5 cm long and has a room temperature resistance of approximately 1.5 Ω. Before deposition, the wires were cleaned with paper towels soaked with acetone and then paper towels soaked with ethanol. To further clean the wires, the wires were heated to ∼800 K in vacuum by passing a DC current through them while monitoring the resistance of the wire. The temperature is determined from the ratio of the resistance of the wire to its value at room temperature. Fig. 12 illustrates the dependence of the temperature on this ratio [57]. Although the melting point of Pt is 2041 K, we have found that the wires would fail if they were heated to a temperature greater than 1000 K because of hotspots on the wire. Most of our wires were heated to 800 K, which corresponds to a resistance ratio of 2.6.

After the frame of wires is mounted in the PLD chamber, the pressure is reduced

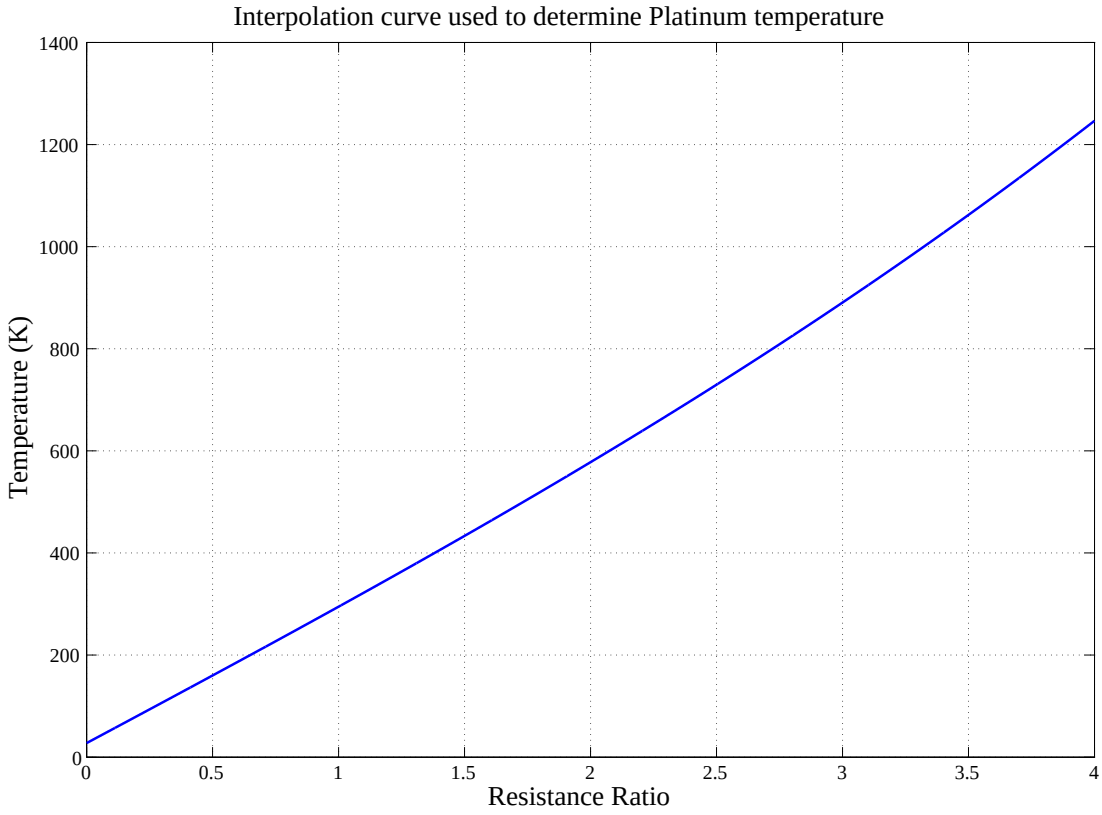

Fig. 12. The temperature of platinum as a function of the ratio of the resistance and the room temperature resistance. From trial and error, we found that the optimum ratio was 2.5 to 2.6, which corresponds to 800 K.

to approximately 10^{-5} Torr. The adjustable decade resistor, R_{decade}, is initially set at its maximum value, 10 kΩ. This resistance is then gradually decreased to 202 Ω at which point the current is approximately 40 mA. At this current, the middle of the heated platinum wire should be a light red. The resistance of the Pt wire should have increased by a factor of 2.6 times from its room temperature resistance. The heating time for each wire is about 15 minutes.

The PLD apparatus is described in detail in reference [34] and therefore we will only give a brief description. Before deposition, the chamber is evacuated with a

diffusion pump to a pressure of 10^{-5} Torr. The source target consists of a pellet made by compressing Mn_{12}-Ac powder with a pressure of 20 kpsi into a stainless steel holder. A Lambda Physic KrF excimer laser operating at 248 nm generates pulses at a repetition rate of 1 Hz with a pulse width of 10 ns. The laser is focused onto a 0.25 cm^2 area and the laser fluence at the target was varied between 200 and 450 mJ. To prevent excessive heating of the Mn_{12}-Ac, the source target was rotated continuously. The distance between Mn_{12}-Ac target and the wires to be coated was approximately 6 cm. The thickness of the deposited film was measured by a quartz crystal microbalance (QMB). When a thickness of 2 monolayers was reached, the wires were then rotated 180° in order to deposit 2 monolayer on the opposite side of the wires. All depositions were made at room temperature. Although the chamber pressure prior to deposition was $\sim 10^{-5}$ Torr, during the pressure deposition, the pressure would vary between 10^{-5} Torr and 10^{-1} Torr. Typical deposition times were approximately 1 min.

3. Dip and Dry (DAD) Method for Deposition of the Mn_{12}-Ac Film

The Dip and dry method is relatively simple and reliable [35]. To produce an 8.7×10^{-4} mol L^{-1} suspension, 18 mg of Mn_{12}-Ac powder is dissolved in 10 mL of isopropanol ($CH_3CHOHCH_3$). Both manual agitation and sonification for a few minutes was used to homogenize the distribution of the suspension in the solvent.

The platinum wires were first cleaned with acetone and methanol. They are dipped into the suspension and then allowed to naturally dry in air at room temperature. This procedure will coat the wires with about one or two monolayers[35].

B. Experimental Procedure

1. Data Acquisition Apparatus and Principles

In order to simultaneously measure the I, dI/dV, and d^2I/dV^2 of the tunnel junction, one can modulate the applied bias voltage at a frequency, ω, and detect the response of the tunneling current at the fundamental frequency, ω, and the second harmonic, 2ω. A schematic of the circuit is shown in Fig. 13.

To understand how the derivative signals are measured, consider expanding $I(V)$ in a Taylor series about $V = V_{DC}$, where the bias voltage is given by $V = V_{DC} + \Delta V \cos(\omega t)$, where ΔV and ω are the amplitude and frequency of AC modulation respectively. In the following, the amplitude of the modulation, ΔV, must be much smaller than the applied DC voltage, $\Delta V \ll V_{DC}$. To second order in the modulation voltage, the tunneling current becomes

$$I(V) = I(V_{DC}) + \Delta V \cos(\omega t) \left.\frac{dI}{dV}\right|_{V=V_{DC}} + \frac{1}{2!} \left[\Delta V \cos(\omega t)\right]^2 \left.\frac{d^2I}{dV^2}\right|_{V=V_{DC}} \tag{2.1}$$

where the ω and 2ω terms are proportional to the first and second derivatives of the junction current $I(V)$ with respect to the bias voltage V. In addition to these terms, there exists a current due to the stray capacitance in parallel with the junction (Fig. 13) that arises from the proximity of the current and voltage leads connected to the junction wires on the SATJ mount. The magnitude of this capacitance is typically about 10^{-13} F. Although this capacitance is small, the corresponding impedance at our nominal operating frequency of 555 Hz is about 3 GΩ. Because the junction resistances range from 10 kΩ to 5 $G\Omega$, it cannot be ignored. The current due to this stray capacitance is given by

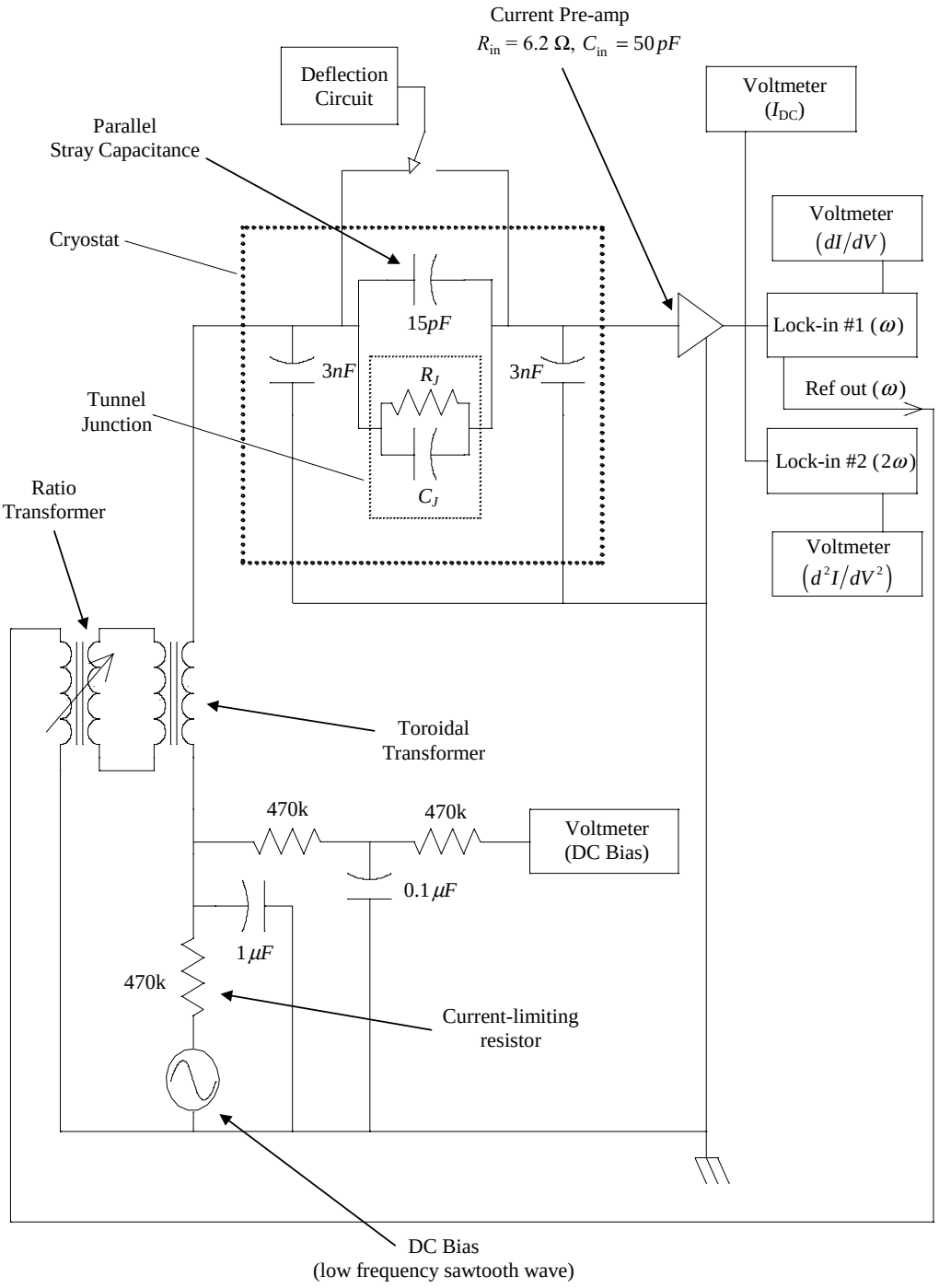

Fig. 13. Circuit schematic showing the basic elements of the signal detection [10].

$$I_C = C\frac{dV}{dt} = C\frac{d}{dt}\left[V_{DC} + \Delta V\cos(\omega t)\right] = -\omega C\Delta V\sin(\omega t) \tag{2.2}$$

Rewriting the third term in equation Eq. (2.1) using the common double-angle identity $\cos^2(\omega t) = \frac{1}{2}\left[1+\cos(2\omega t)\right]$ and using the fact that in Eq. (2.2), $-\sin(\omega t) = \cos(\omega t + 90^\circ)$, we have for the total current,

$$\begin{aligned} I(V) &= I(V_{DC}) + \Delta V\left[\cos(\omega t)\left.\frac{dI}{dV}\right|_{V=V_{DC}} + \omega C\cos(\omega t + 90^\circ)\right] \\ &\quad + \frac{\Delta V^2}{4}\left[1+\cos(2\omega t)\right]\left.\frac{d^2I}{dV^2}\right|_{V=V_{DC}} \end{aligned} \tag{2.3}$$

The first term in this expansion corresponds to the DC tunneling current. The second term corresponds to the differential conductance ($G \equiv dI/dV$) and the capacitive AC current whereas the third term is proportional to the IETS signal (d^2I/dV^2).

The DC bias voltage is typically ramped between -0.7 V and +0.7 V using a sawtooth wave with frequency 1/7200 sec^{-1} provided by an HP 3245A synthesizer function generator. The DC tunneling current is read directly from a current sensitive pre-amplifier (EG&G/PARC Model 184) that is powered by the first lock-in amplifier (LIA1). The pre-amp has a sensitivity ranging from 10^{-5} to 10^{-9} A/V, but because of residual noise in the SATJ circuit that tends to overload the LIAs, we do not normally operate below the 10^{-5} A/V setting. The pre-amp converts the tunneling current to a voltage that is read by an HP 3457A voltmeter. The input to this pre-amp is offset from ground which results in an offset voltage of -9.5414 mV at zero tunneling current. This offset voltage must be subtract from the current measurements before analyzing the data.

The AC component normally has a frequency of 555 Hz and an rms amplitude between 5-20 mV. LIA1 provides the AC component and is set to detect the response

at ω which is proportional to (dI/dV). The capacitive term in Eq. (2.3) will be rejected by LIA1 because it is shifted 90° with respect to the first derivative signal. The second lock-in amplifier (LIA2) measures the response at 2ω which is proportional to (d^2I/dV^2). Both units are EG&G/ PARC Model 124A. The AC signal for each LIA is filtered by the internal band-pass filters to remove unwanted side-band noise.

The DC ramp and the outputs from the preamp and LIAs are recorded by a 4 channel Tektronix TDS 460A oscilloscope connected to the computer via an ICS Electronics IEEE 488 Bus Extender Model 4887A [58]. LabVIEW programs were developed to initiate the bias voltage sweep and to acquire and process the data. Graphs of the data together with all the setup information was plotted using PLOT routines.

The raw data read by the oscilloscope must be appropriately scaled to give the correct values for the three quantities of interest. To determine the DC tunneling current, the voltage offset from the pre-amp is first subtracted from the recorded DC output of the current pre-amp. This voltage is then multiplied by the pre-amp sensitivity (in A/V).

The junction conductance ($G = dI/dV$) is calculated from the output of LIA1 via

$$\frac{dI}{dV} = \frac{(V_{LIA1})(AC_{sensitivity})(DC_{sensitivity})}{10(V_{AC})_{rms}}$$

where V_{LIA1} is the DC output of the LIA1 and $(V_{AC})_{rms} = \Delta V/\sqrt{2}$. $AC_{sensitivity}$ and $DC_{sensitivity}$ refer to the AC gain setting on the LIAs and the DC pre-amp gain setting, respectively. The factor of 10 in the denominator is due to the fact that the full scale output of the LIAs is $10\,V$. The IETS signal (d^2I/dV^2) is similarly given by

$$\frac{d^2I}{dV^2} = \frac{2\sqrt{2}(V_{LIA2})(AC_{sensitivity})(DC_{sensitivity})}{10(V_{AC})^2_{rms}}$$

where the $2\sqrt{2}$ factor is due to the coefficients that appear in the Taylor expansion (Eq. 2.3) and the trigonometric identities used therein.

2. Forming Junction and Data Acquisition

The experimental details from soldering the junction wires, cooling down the cryostat to liquid helium temperature, leak detection, stray capacitance measurement, dosing barrier gas, to choosing the correct phases of LIAs and adjusting the deflection current and magnetic field to form a junction are all described in Dr. D. Zimmerman's thesis [10] so I will only give a brief description of the procedures.

1. Solder a bare wire ($\sim$ 1.5 cm long, Pt, Al, Fe, ...) to the copper posts on the mount that will serve as the straight wire. Solder two wires coated with Mn_{12}-Ac to the copper posts for the curved wires. Make sure that the distance between the straight wire and the curved wires is approximately 1 mm. Seal the vacuum can to the cryostat with a lead o-ring made with Buss wire #2 [59].

2. Move the cryostat into the shielded room and connect it to the helium leak detector. Make all the connections for measuring the temperature, current, and voltages. Attach the leads to the magnetic coil. Connect the cryostat to the neon gas tank. Use the leak detector to test for leaks in the cryostat. If no leak is found (the leak rate should be below 5×10^{-8} atm cm^3s^{-1}), compare all the measured resistances to those measured in previous cooldowns. Nominal values of these resistances at room temperature, liquid nitrogen temperature, and liquid helium temperature, are listed in Table I, II, and III. Here the critical step is to make sure that the 3 junction wires are properly soldered on the

electrical posts and that there are no electrical shorts.

3. Measure the stray capacitance by using frequency ω and determine the phase of LIA1 such that the maximum signal is obtained, and then add an additional 90° so that the LIA will reject the stray capacitance signal and measure only the signal that arises from tunneling. Use the same method for LIA2 and frequency 2ω to find the right phase for LIA2 (but this time 180° should be added because there is 90° difference between the reference frequencies of LIA1 and LIA2). These two measurements of the capacitance should agree and be on the order of 10^{-13} F. Setting the phase correctly is critical in order to obtain the correct 1st and 2nd derivatives of the current. Nominal values of the phases are: LIA1: 90°+86.8°, LIA2: 180°+88°; The nominal values of the capacitance are: $C(\omega) = 2.80\times10^{-13}$ F and $C(\omega) = 5.81\times10^{-13}$ F.

4. Run the LabVIEW program "Paros_2.vi" to monitor the neon pressure inside the 2L storage container and keep the pressure above 1 kTorr.

5. Flush the cryostat with neon 5 times and leave $\sim$ 200 mTorr neon inside; flush the 1 K pot with helium 5 times and pressurize the 1 K pot with helium at $\sim$ 15 psi (relative pressure).

6. Immerse the cryostat into liquid nitrogen. After it cools down to liquid nitrogen temperature ($\sim$ 2 hours), measure all resistances and compare them with those measured in previous cooldowns.

7. Open the valve to the vacuum can and pump all the neon out. Immerse the cryostat into liquid helium dewar gradually. Monitor the leak detector to see whether a leak has developed during the cooldown. If no leak is found, close the valve to the vacuum can.

8. After the cryostat cools down to liquid helium temperature (∼2 hours), measure all resistances again and compare them with those measured in previous cooldowns. Notice that the resistances of the junction wires should be greatly reduced compared to their values at liquid nitrogen temperature.

9. Now the critical part – forming the junctions. Slowly increase the deflection current to about 25 mA (corresponding to a voltage of 2.5 V on the power supply). Turn on the power supply for the superconductor magnetic and gradually increase the magnetic field until the junction is formed. This can be verified by the voltage reading of the pre-amplifier. The output of the pre-amplifier should change from its background value of -9.50 mV to a value more negative than -11 mV. The actual value will depend on the bias voltage and thickness of the barrier film. If the junction has an electrical short then the output voltage of the pre-amplifier will either be positive or have a value more negative than -3 V. If this should occur, break the contact by reducing the magnetic field and try again. If the electrical short persists, add more neon gas to the cryostat. For the procedure of adding gas to cryostat please refer to Chapter 3 in the thesis of Dr. D. T. Zimmerman [10]. If the junction cannot be formed, check to see whether there are any electrical shorts in the wires. If no other problems are found, raise the cryostat out of the helium bath so that some of the neon plated on the walls can return to the gas phase. When the cryostat is cooled, more neon will be deposited on the wires.

10. Run the LabVIEW program "Program to Initialize 3245A.vi" to initiate the parameters for the synthesizer function generator (HP 3245A); run "Initiate Sweep.vi" to start a voltage sweep.

11. After the voltage sweep is finished, run "SATJ_MASTER_PROG.vi" to down-

load the data from the Tektronix oscilloscope to the computer. Pay attention to the comparison between the recorded I and the one obtained by integrating the dI/dV data, and the recorded dI/dV and the one obtained by integrating d^2I/dV^2. If they do not match, center frequencies or phases of the two LIAs may need an adjustment.

12. Run PLOT program "new_std.plt" to plot and print the I-V , dI/dV-V, and d^2I/dV^2-V curves.

Tables I, II and III, list the nominal values of the resistances at different temperatures. Each wire terminal is identified by either a letter or a number . For example, the four terminals for the 1 K Pot heater are: R, S, T, and U. The terminals of the platinum junction wires are labeled from 1 to 10 and C and D.

Table I. Nominal resistance values at room temperature

Time: 6:00pm	Temperature: Room	Date: 08/16/04
Experimenter: Lianxi Ma	Bath Thermometer: 518 Ω	E-F Capillary heater, 2 wires: 151 Ω

1-K Pot Heater (133.36 Ω)

T-R	312 Ω	R-S	312 Ω
T-S	179 Ω	R-U	179 Ω
T-U	312 Ω	S-U	312 Ω

Germanium Thermometer (1.69 Ω)

M-N	182 Ω	N-L	182 Ω
M-L	181 Ω	N-P	182 Ω
M-P	182 Ω	P-L	183 Ω

Capillary Thermometer (1.017 kΩ)

G-H	1.195 kΩ	H-J	0.179 kΩ
G-J	1.195 kΩ	H-K	1.195 kΩ
G-K	0.179 kΩ	J-K	1.195 kΩ

Junction Wires

Straight wire: 5.70 Ω		Bottom curved wire: 2.79 Ω		Top curved wire: 3.482 Ω	
9-7: 103 Ω	7-8: 36 Ω	5-4: 99 Ω	4-6: 101 Ω	10-2: 181 Ω	2-C: 97 Ω
9-8: 111 Ω	7-1: 110 Ω	5-6: 180 Ω	4-3: 23 Ω	10-C: 112 Ω	2-D: 115 Ω
9-1: 184 Ω	8-1: 103 Ω	5-3: 102 Ω	6-3: 99 Ω	10-D: 100 Ω	C-D: 34 Ω
Type: Pt		Type: Pt+Mn_{12}-Ac		Type: Pt+Mn_{12}-Ac	

Table II. Nominal resistance values at liquid nitrogen temperature

Time: 11:10pm	Temperature: LN2	Date: 08/16/04
Experimenter: Lianxi Ma	Bath Thermometer: 611 Ω	E-F Capillary heater, 2 wires: 150 Ω

1-K Pot Heater (130.67 Ω)

T-R	306 Ω	R-S	307 Ω
T-S	176 Ω	R-U	176 Ω
T-U	307 Ω	S-U	307 Ω

Germanium Thermometer (2.32 Ω)

M-N	181 Ω	N-L	181 Ω
M-L	178 Ω	N-P	178 Ω
M-P	181 Ω	P-L	180 Ω

Capillary Thermometer (1.360 kΩ)

G-H	1.533 kΩ	H-J	0.176 kΩ
G-J	1.533 kΩ	H-K	1.534 kΩ
G-K	0.176 kΩ	J-K	1.534 kΩ

Junction Wires

Straight wire: 3.052 Ω		Bottom curved: 0.601 Ω		Top curved wire: 0.639 Ω	
9-7: 97 Ω	7-8: 27 Ω	5-4: 90 Ω	4-6: 90 Ω	10-2: 168 Ω	2-C: 101 Ω
9-8: 98 Ω	7-1: 100 Ω	5-6: 90 Ω	4-3: 16 Ω	10-C: 101 Ω	2-D: 90 Ω
9-1: 169 Ω	8-1: 93 Ω	5-3: 91 Ω	6-3: 91 Ω	10-D: 90 Ω	C-D: 23 Ω
Type: Pt		Type: Pt+Mn_{12}-Ac		Type: Pt+Mn_{12}-Ac	

Table III. Nominal resistance values at liquid helium temperature

Time: 10:50 Am	Temperature: LHe	Date: 08/17/04
Experimenter: Lianxi Ma	Bath Thermometer: 981 Ω	E-F Capillary heater, 2 wires: 144 Ω

1-K Pot Heater (120.6 Ω)

T-R	290 Ω	R-S	290 Ω
T-S	169 Ω	R-U	169 Ω
T-U	290 Ω	S-U	290 Ω

Germanium Thermometer (60.97 Ω)

M-N	250 Ω	N-L	251 Ω
M-L	192 Ω	N-P	193 Ω
M-P	252 Ω	P-L	252 Ω

Capillary Thermometer (13.60 kΩ)

G-H	27.7 kΩ	H-J	0.171 kΩ
G-J	28.0 kΩ	H-K	28.1 kΩ
G-K	0.170 kΩ	J-K	28.2 kΩ

Junction Wires

Straight wire: 2.168 Ω		Bottom curved wire : 0.108 Ω		Top curved wire: 0.007 Ω	
9-7: 76 Ω	7-8: 15 Ω	5-4: 78 Ω	4-6: 78 Ω	10-2: 144 Ω	2-C: 87 Ω
9-8: 85 Ω	7-1: 77 Ω	5-6: 144 Ω	4-3: 14 Ω	10-C: 87 Ω	2-D: 78 Ω
9-1: 146 Ω	8-1: 83 Ω	5-3: 79 Ω	6-3: 80 Ω	10-D: 78 Ω	C-D: 19 Ω
Type: Pt		Type: Pt+Mn_{12}-Ac		Type: Pt+Mn_{12}-Ac	

CHAPTER III

EXPERIMENTAL RESULTS

A. Junctions Formed with Pure Neon

To characterize the behavior of SATJs, we examined junctions in which neon was used for the tunneling barrier. Neon is a good choice for the barrier because even at liquid helium temperature, the neon solid is still fairly compressible, making it possible to change the thickness of the barrier and thereby the resistance of the junction. (The triple point temperature and pressure of neon are 24.553 $\pm$ 0.001 K, and 43332 $\pm$ 13 N/m^2 [60].) In addition, the first excitation energy of neon is 16.6 eV [61] so the interaction between the tunneling electrons and this state can be ignored. We expect that the current for such junctions should be described by the simple tunneling theory discussed in Chapter I.

The current and conductance data for a Pt+Fe/Ne/Pt junction are shown in Fig. 14. The three curves were all from one junction, showing that they are very reproducible. By fitting the data to Eq. (1.15), we should be able to determine the thickness and contact area of the junction. Although the fit in Fig. 14(d) looks good, the parameters determined by the fit are unreasonable. For example the work function of the platinum had to be reduced to a value between 1.5 and 2 eV rather than the published value of 5.65 eV [62], or 6.35 eV[63]. With these values for the work function, the thickness of the barrier is approximately 22 Å. This value for the thickness greatly suppresses the overall current in the junction, so to compensate the area of the junction becomes on the order of 2×10^{-12} m^2. Because the wire diameter is only 25 μm, this area is far too large. One possible explanation is that the expressions derived in Chapter I are not appropriate for such a large voltage

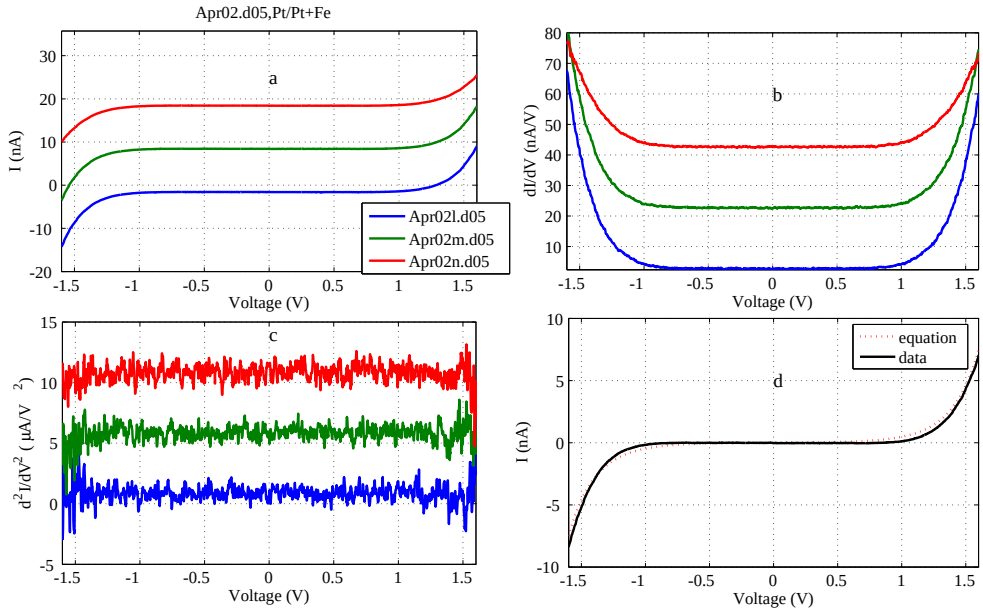

Fig. 14. I (a), dI/dV (b), and d^2I/dV^2 (c) data for Pt+Fe/Ne/Pt junctions. A comparison between the current and theory is shown in (d). For clarity, the data for Apr02m.d05 and Apr02n.d05 have been shifted in (a) by 10^{-8} A and 2×10^{-8} A, in (b) by 2×10^{-8} A/V and 4×10^{-8} A/V and in (c) by 5×10^{-6} A/V^2 and 1×10^{-5} A/V^2 respectively.

range. To see whether the analysis can be done in the region near zero bias voltage, the maximum bias voltage was reduced from 2 V to 0.5 V (Fig. 15).

As discussed in Chapter I, in the limit that the bias voltage is small compared to the work function φ, the conductance of the junction can be expanded in powers of the bias voltage. As shown in Eq. (1.18), the conductance should depend quadratically on the bias voltage. We analyzed three data sets, Feb09G.d01, Feb09H.d01, and Feb09I.d01 shown in Figs. 15(a), (b), and (c). Using 5.56 eV for the work function of platinum we can fit Feb09I.d01 with a value of s=17 Å, which agrees with the previous values for the thickness. If we however calculate the conductance at zero bias, we must use a value for the area that is much larger than the cross-section of the wire. This may indicate that the work function of the platinum is in fact suppressed

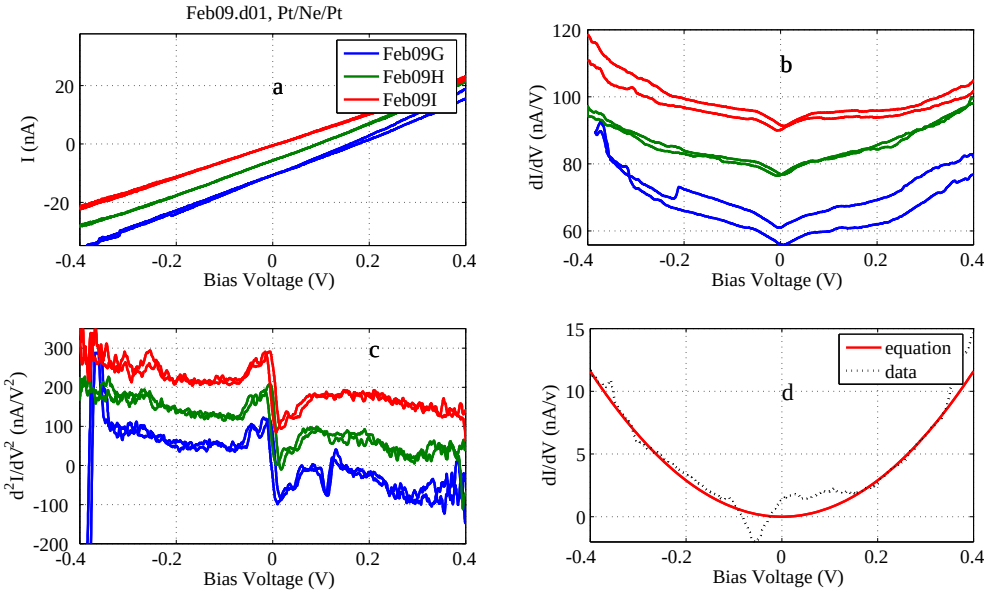

Fig. 15. Current (a), conductance (b) and IETS (c) data from Pt/Ne/Pt junctions. In (d), a fit to the quadratic dependence of the conductance on the bias voltage is shown. The region of the zero bias feature near $V = 0$ was excluded from the fit.

or that the simple tunneling theory must be modified. One possible extension would be to include image effects [42], [44].

The conductances in Fig. 15(b) and (d) also show a marked suppression of the conductance in the region of zero bias voltage. This zero bias feature (ZBF) is observed in most of our data. In the region of the ZBF, the conductance scales as $V^{1/2}$ if V is not very close to zero. Agnolet et al. [64] were able to fit this region of the data with a two-channel Kondo model (2CK) [65]. In this model the conduction can be expressed as $G(V,T) = G(0,T) + BT^{1/2}\Gamma(Av)$ where $v = (eV/k_BT)$ and A and B are scaling parameters. The universal scaling function, $\Gamma(v)-1$ asymptotically approaches $v^{1/2}$ as $v \to \infty$. They found that at liquid helium temperature, A=0.36 and B=0.0031 $\mathrm{K}^{-1/2}e^2/h$.

In the next section, we discuss the results when irons atoms were deposited onto the platinum wires. By introducing magnetic atoms, one would expect an enhanced Kondo effect. These results will be compared with the data from the bare platinum wires.

B. Pt+Fe/Ne/Pt Junctions

To test whether one could enhance the ZBF, iron was evaporated directly onto the surface of the platinum wires. The thickness of the iron was less than a monolayer. Some results are shown in Fig. 16. The observed ZBFs in the region $|V|$ <0.05 V, appear more pronounced than those observed in the Pt/Ne/Pt junctions shown in Fig. 15. The average height of the ZBF for the bare wires is approximately 10^{-9} A/V, whereas the average height of the ZBF for iron coated platinum wires is approximately 10^{-8} A/V. Furthermore, the ZBFs do not appear to be symmetric because the positions of the shoulders for $V > 0$ are different from those in the $V < 0$ region.

Interestingly, we found that the character of the ZBFs could change for subsequent voltage sweeps. The data in Fig. 17 is for a single junction and shows that the ZBF changes from a dip to a peak and then back to a dip again. Fig. 18 shows the ZBFs for the low conductance curves on an enlarged scale. An analysis of the ZBFs in terms of the two-channel Kondo model will be discussed in Chapter IV.

C. Pt/Mn_{12}-Ac/Pt Junctions Formed with Fresh Mn_{12}-Ac Films

Because we found no significant difference between the tunneling results of Mn_{12}-Ac film deposited by PLD and DAD, the data from both types of junctions will be discussed as a group.

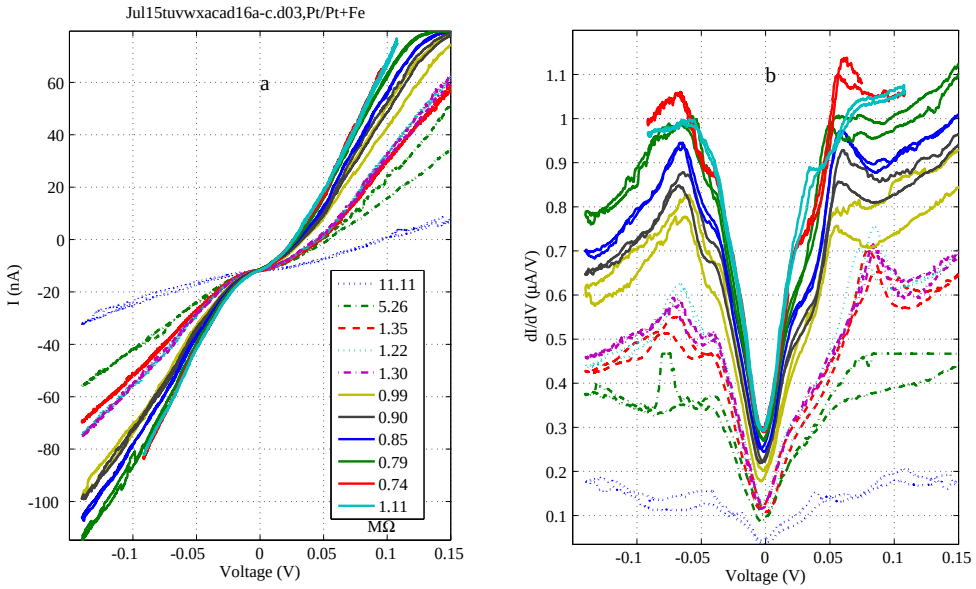

Fig. 16. Current (a) and conductance (b) of a Pt+Fe/Ne/Pt junction.

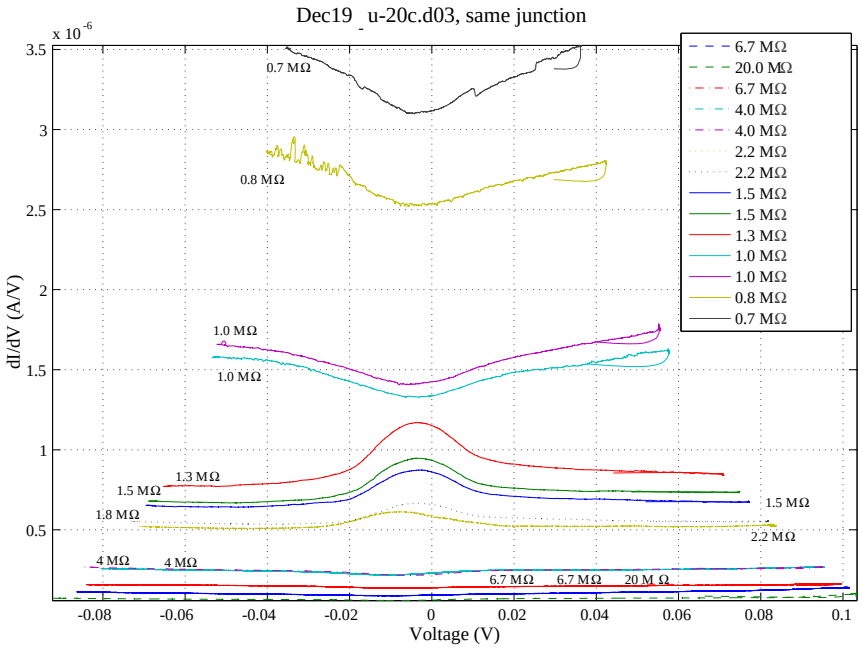

Fig. 17. Data from a single Pt+Fe/Ne/Pt junction showing that the ZBF can change from a dip to a peak and then back to a dip again. The curves are shifted because the conductance of the junction increased as a function of time.

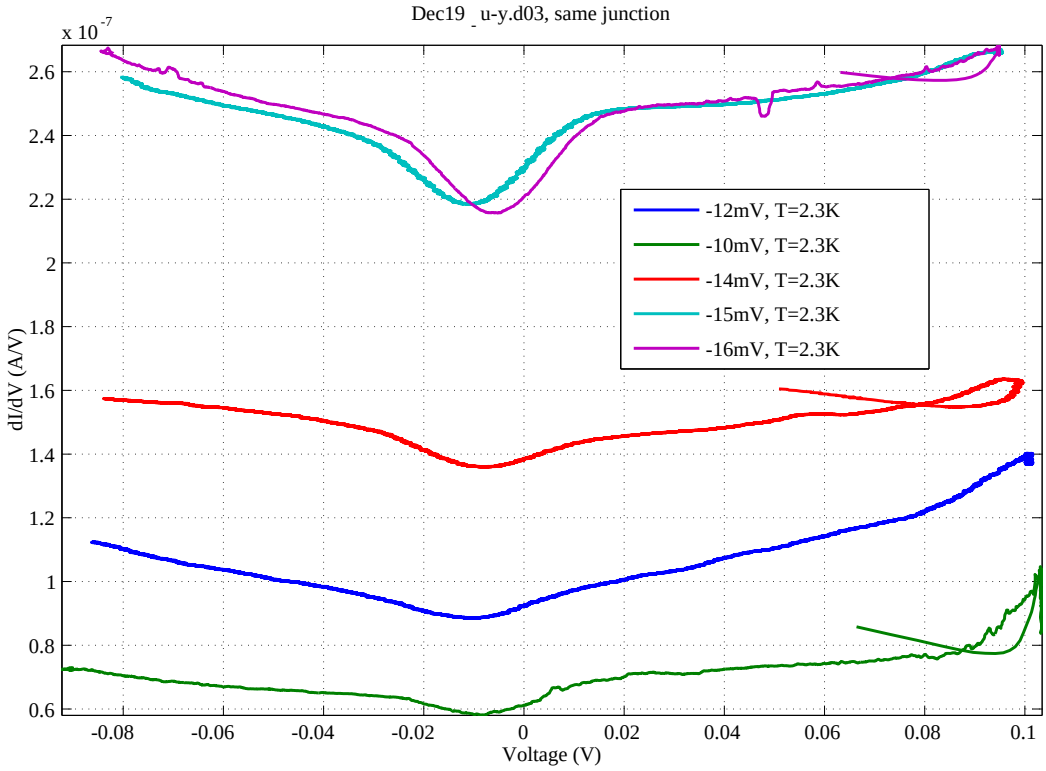

Fig. 18. An expanded view of the data from a Pt+Fe/Ne/Pt junction with low conductances. The curves are shifted because the conductance of the junction increased as a function of time.

As with the bare Pt/Ne/Pt junctions, a ZBF was often observed for these Pt/Mn_{12}-Ac/Pt junctions. Examples of the current and conductance of these junctions are shown in Fig. 19. The ZBFs in high resistance junctions were typically dips in the conductance. However, as the initial resistance decreases, we observed the gradual change of the ZBF from a dip to a peak. It is also worth noting that sometimes even when all the parameters of the sweep (magnetic field, deflecting current, V_{max}, sweep time, AC modulation) remained the same, a dip can change to a peak in a subsequent sweep. This behavior can be seen in Fig. 19b in which all of the data except the black one were taken from one junction. The black one is more

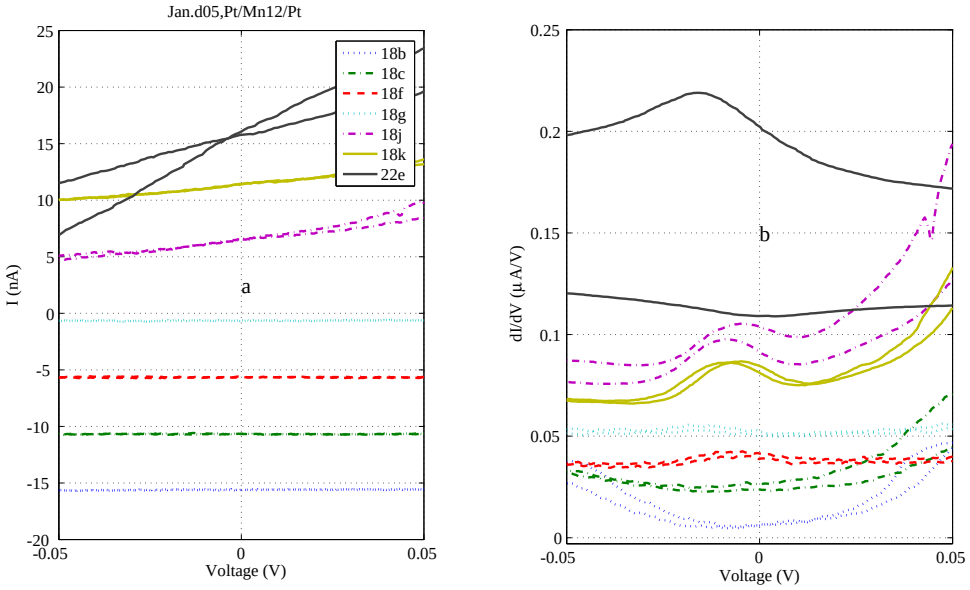

Fig. 19. Current (a) and conductance (b) data for Pt/Mn_{12}-Ac/Pt junctions. The ZBF gradually changes from a dip to a peak as the resistance of the junctions decreases. Data 18b, c, f, g, j, k are all from the same junction. For clarity, the curves have been offset and magnified. The magnification factors are 5×10^7 (18 b and c), 10^8(18f), 3×10^8 (18g), 8×10^6 (18j) and 5×10^6 (18k). The actual conductances range from 0.1 μA/V to 1 μA/V.

interesting because the dip which is observed when the bias voltage is swept from from $+V$ to $-V$ changes to a peak when the voltage sweep is reversed. Because it is highly unlikely that this behavior is caused by a change of the tunnel barrier thickness, we assume that it is caused by a change in the molecular configuration induced by the current or bias voltage. Gregory [14] observed similar transitions in his SATJs in which the wires were tungsten and helium was used for the junction barrier. In his experiments, the ZBF would change from a dip to a peak as the magnetic field was increased. He attributed this to the scattering of the conduction electrons from a single localized magnetic moment. However, Gregory did not report observing this transition in junctions made with platinum wires and helium. In our experiments,

the ZBF and the transition from the dips to peaks were also observed in junctions with different metal wires (such as Fe, Al) and different tunnel barriers (such as C60, Ne).

Another interesting phenomenon is observed in 7.1% out of a total 509 data sets. In these "state jumps", the differential conductance suddenly switches from one value to another at specific voltages. In Fig. 20, some of these state jumps are displayed. These jumps can occur either as the bias voltage increases or decreases and may either be positive or negative. These jumps often occur at $V \sim$ -0.1 V. However, if the state jump does occur at a positive bias voltage, it usually appears at a random bias voltage. This asymmetry maybe due to an anisotropy of the Mn_{12}-Ac molecules. Heersche et al. [66] also observed this type of asymmetry in their transport measurements of the Mn_{12} derivative, $[Mn_{12}O_{12}(O_2C\text{-}C_6H_4\text{-}SAc)_{16}(H_2O)_4]$, in a single-molecule transistor geometry. They did not give an explanation though.

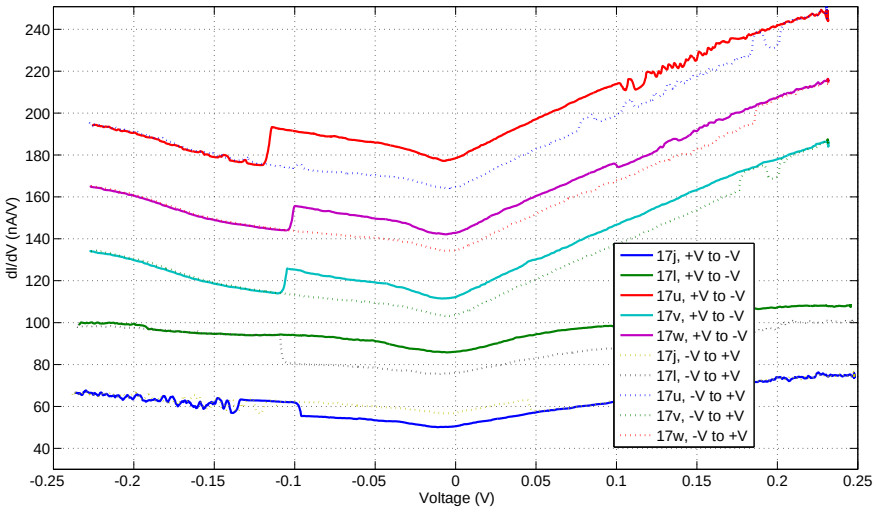

Fig. 20. Conductance jumps near $V = -0.1$ V may indicate a configurational change of the $Mn_{12} - Ac$ molecules. The jumps can be either positive or negative and can occur during a positive or negative voltage sweep. Note that the ZBFs are still present. The curves have been offset for clarity.

We have also observed a "staircase" pattern in the $I - V$ traces as shown by the blue curve in Fig. 21. This behavior can be seen more clearly by plotting the conductance versus the bias voltage (red curve). While this phenomenon is more typical in single molecule tunneling devices [67] [68] [69] [70], it is only rarely seen in our device (only 2.55% of the 509 data sets). We have found that to have a good staircase pattern, the bias voltage should not exceed ± 2 V, the sweep rate should

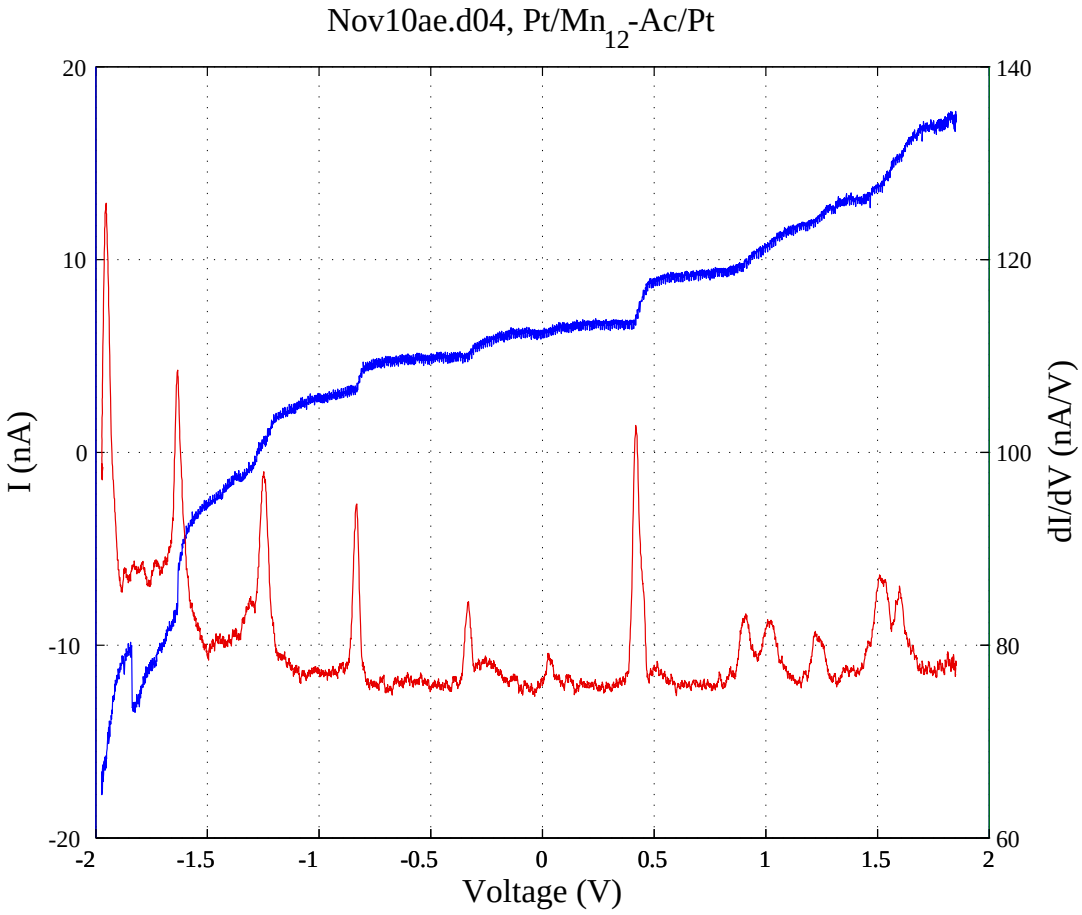

Fig. 21. "Staircase" pattern. At regularly spaced bias voltages, the current (blue) increases suddenly. In between these steps the current remains almost constant. The differential conductance (red) shows peaks corresponding to the current steps.

not be slower than 6.4 mV/s and the initial resistance should be around 10 MΩ. In addition, this phenomena was only observed if the Mn_{12}-Ac was freshly deposited.

This type of phenomenon was first observed in a tunnel junction by J.B. Barner and S.T. Ruggiero [71]. They embedded silver particles into a 25 to 40 Å thick Al_2O_3 film separating the metal electrodes. They concluded that the staircase is a manifestation of a collective change in the charge residing on the silver particles and that the charge occupation of the particles is a coherent phenomenon.

The 'staircase" pattern can be understood in terms of Coulomb blockade [72]. In a single tunnel junction, the current is actually discrete due to the tunneling of electrons across the junction under the influence of the bias voltage. The metal-insulator-metal junction can also be treated as a capacitor. When the tunnel junction capacitor is charged by an electron, a voltage, $U = e/C$, appears across the junction where e is the electron charge and C is the capacitance of the junction. If the capacitance is very small, the voltage buildup can be sufficiently large to prevent another electron from tunnelling when the electrons are supplied by a current source. The current is therefore suppressed at low bias voltages and the resistance of the device is no longer a constant. The increase of the differential resistance around zero bias is called the Coulomb blockade.

K. Mullen et al. [73] extended this concept by considering a device consisting of two tunnel junctions in series. Fig. 22 shows a schematic in which the tunnel junctions are represented by two capacitors and two resistors. Based on numerical calculations, they shows that the $I - V$ characteristics depend on the particular values of R_1, R_2, C_1, and C_2. When $R_1 \ll R_2$, and $C_1 < C_2$, they obtained a staircase pattern in the $I - V$ curves. They explained that when a number of electrons, δQ, accumulates on the "island' " between the two capacitors, the Fermi level in the center region changes with δQ even though the circuit is driven by a voltage source. The change in V_1 as

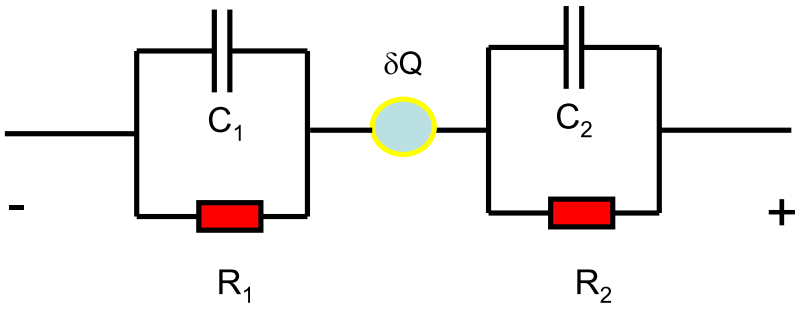

Fig. 22. Schematic representation of a pair of tunnel junctions connected in series, driven by an ideal voltage source

δQ increases by one electron is $e/(C_1 + C_2)$. Correspondingly, the difference between the Fermi energy on the right hand side of the first junction and the energy of the tunneling electron shifts by half of this amount, that is, $e^2/2(C_1 + C_2)$. This shift in the Fermi level inhibits tunneling at voltage below $e/2(C_1 + C_2)$ producing a step in the $I - V$ characteristic.

An increase of the external voltage ΔV_{ex} will increase δQ by one electron,

$$\Delta V_{ex} = \frac{e}{C_2} \tag{3.1}$$

producing a voltage jump, $\Delta V_2 = e/(C_1 + C_2)$, across the second junction with a corresponding increase in the current

$$\Delta I = \frac{\Delta V_2}{R_2} = \frac{e}{R_2(C_1 + C_2)} \tag{3.2}$$

If we average over four of the current steps and the corresponding bias voltages

V_{ex}, we get $\Delta\overline{I}$=1.7 nA, and $\Delta\overline{V_{ex}}$=0.42 V. Substituting the $\Delta\overline{V_{ex}}$ into Eq. (3.1) we obtain $C_2 = 3.81 \times 10^{-19}$ F and an average resistance of $\overline{R} = 2.69 \times 10^8$ Ω. Because of $R_2 \gg R_1$, we approximate R_2 to be 2.0×10^8 Ω. Therefore, substituting $\Delta\overline{I}$ into Eq. (3.2) we obtain that

$$C_1 + C_2 = \frac{1.6 \times 10^{-19}}{2 \times 10^8 \times 1.7 \times 10^{-9}} = 4.7 \times 10^{-19} F$$

and therefore, $C_1 = 4.7 \times 10^{-19} - 3.81 \times 10^{-19} = 9 \times 10^{-20}$ F, which satisfies the condition $C_1 < C_2$.

In our Pt/Mn_{12}-Ac/Pt junctions, a single Mn_{12}-Ac molecule could act as an isolated "island" between the two wires. During a tunneling process, an electron could reside on the molecule. If the conditions $R_2 \gg R_1$, and $C_1 < C_2$ are satisfied,then one should observe a staircase pattern.

According to reference [73], care must be taken to align the Fermi levels of the "islands" by first holding the potential constant between the two electrodes. To observe the steps clearly, the voltage must be swept at a rate faster than the "islands" can alter their alignment. This is confirmed in our experiment because the staircase pattern is never observed when the sweep rate is slower than 2 mV/s .

D. Junction Formed with Mn_{12}-Ac Stored for 6 Months

After the deposition of Mn_{12}-Ac on the platinum wires, we used two of the wires to carry out the experiments described above. We stored the other coated wires in a vacuum chamber ($\sim 10^{-2}$ Torr) for 6 months and then repeated the above measurements. In general, these junctions exhibited random switching of varying frequencies, amplitudes, and positions.

Fig. 23 shows a typical result (82.7% out of 110 data sets corresponding to 22

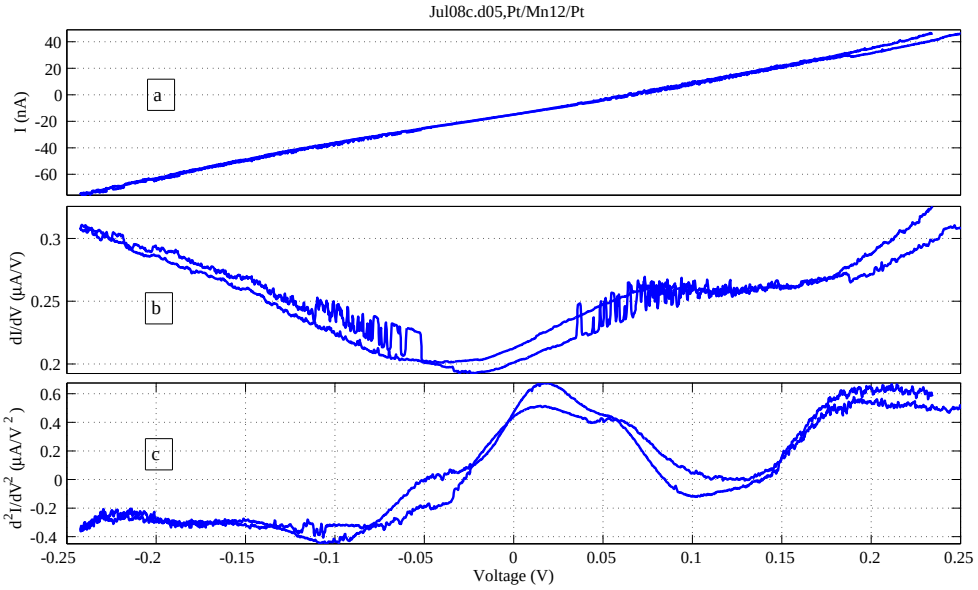

Fig. 23. Results from a Pt/Mn_{12}-Ac/Pt junction in which the Mn_{12}-Ac had been stored in vacuum for 6 months. Although the current data (a) is similar to that observed for junctions made with fresh Mn_{12}-Ac, the dI/dV (b) and d^2I/dV^2 (c) data show random switching and hysteresis.

different junctions). The bias voltage sweep time is 2000 s and 1 mV/s. We noticed that the hysteresis in dI/dV vs. V and d^2I/dV^2 vs. V persists even though the bias voltage sweep rate was decreased to the longest sweep time 2000 s. This switching occurs even in the very low voltage region. As can be seen from Fig. 24 in which data was recorded as a function of time at constant bias voltage ($V = 0.2$ V), the switching is not a result of the changing voltage but due to fluctuations in time.

We believe that this switching behavior is due to the presence of electron traps in the tunnel barrier[74]. According to Ref. [74], it is suggested that the traps are microscopic systems in which atomic rearrangements cause trapping and ejection of electrons. These systems have two available configurations, associated with which are two coupled potential wells. Transitions between the two configurations will be ther-

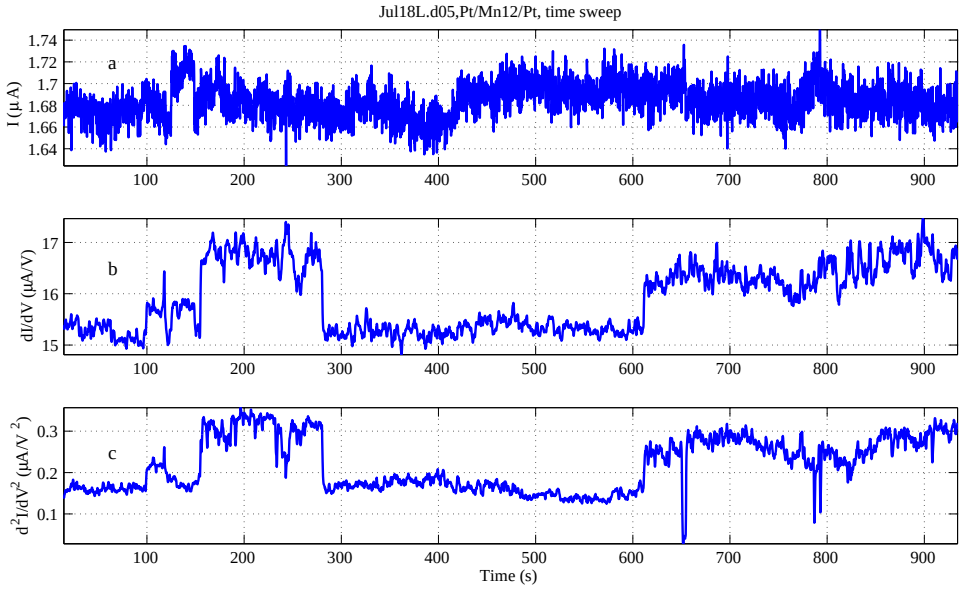

Fig. 24. Switching noise in the current (a), conductance (b) and d^2I/dV^2 (c) as a function of time at a bias voltage $V = 0.2$ V.

mally activated at high temperatures whereas at low temperatures atomic tunneling may take place. Since the process is random and the charge fluctuation modulates the tunnel barrier, the conductance should display "telegraph" or "switching" noise similar to that seen in Fig. 24. The large number of electron traps in the stored Mn_{12}-Ac molecules suggests that over time the molecules may have decomposed into small molecules.

Because the "staircase" pattern is easily distinguishable, we also tried to see whether it could also be observed in junctions made with Mn_{12}-Ac that had been stored for 6 months. The best example is shown in Fig. 25 where that staircase shape can be barely be seen even at low bias voltages. The corresponding peaks in conductance are ambiguous.

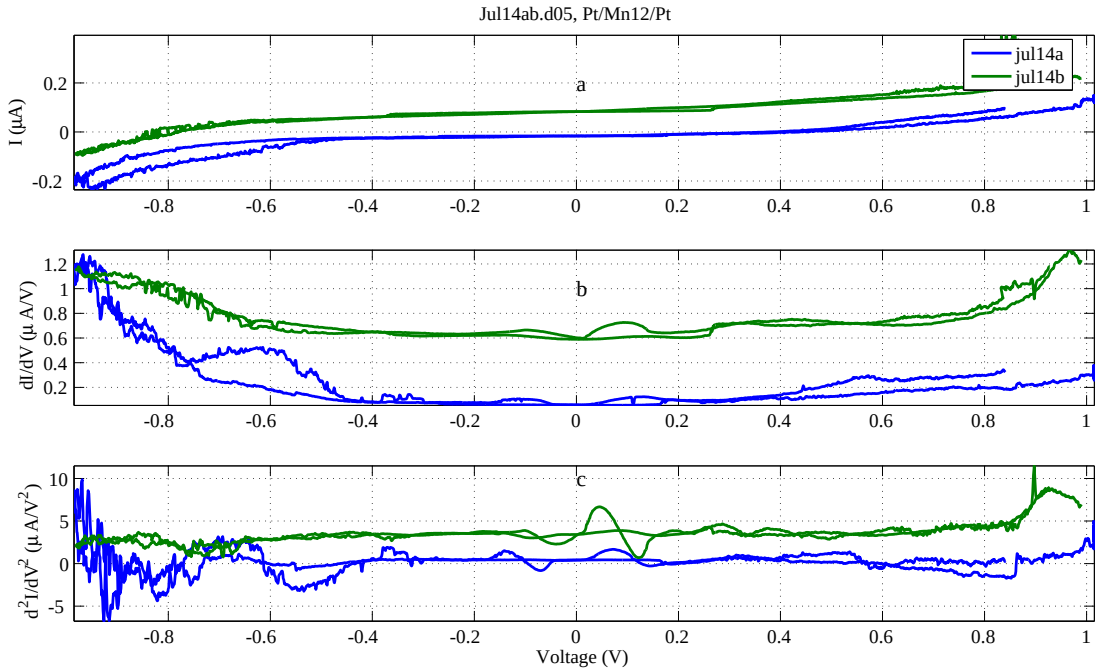

Fig. 25. The current (a), conductance (b) and d^2I/dV^2 (c) of a junction made with Mn_{12}-Ac that had been stored for 6 months. The staircase pattern is no longer obvious and the corresponding peaks are ambiguous. The curves have been offset for clarity.

E. Al/Mn_{12}-Ac/Al Junctions

With the DAD method, we also deposited Mn_{12}-Ac on pure aluminum wires (diameter 0.001 inch with 99.99% purity [75]) and measured the conductance of these films. Because there is a natural oxide layer on the aluminum surface [76] [77], the junction should behave as an equivalent electrical circuit of two capacitors in series and therefore, according to Ref. [73], the $I-V$ curves should exhibit a Coulomb blockade staircase. Typical results for these junctions are shown in Fig. 26. We can see that although there are steps on $I-V$ curves, they are different from those observed in the Pt/Mn_{12}-Ac/Pt junctions because after each jump, the current continues to increases

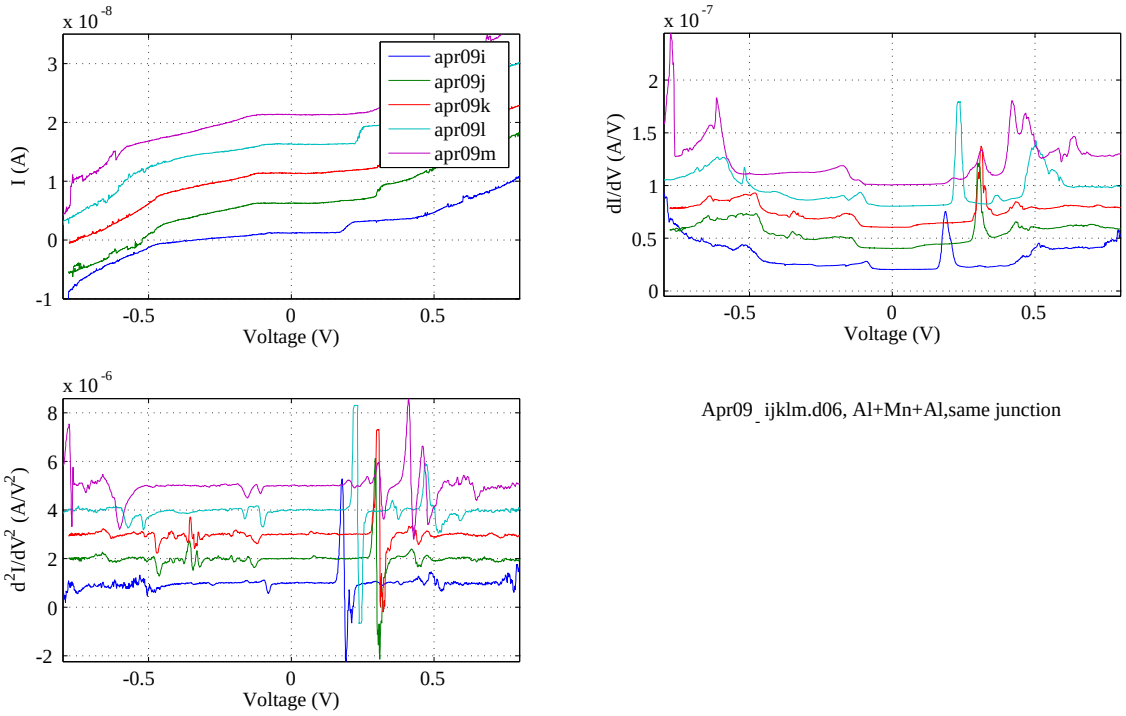

Fig. 26. Typical results of SATJ with Al/Mn_{12}-Ac/Al. The staircase form of $I - V$ characteristics seem to exist but they are different from those of Pt/Mn_{12}-Ac/Pt. The curves have been shifted for clarity.

with V. We believe that the films formed by the DAD method are more uniform than those formed by the PLD method. Therefore, the tunneling current in films made with DAD may be averaging over more molecules and thereby reducing the Coulomb blockade effect associated with a single molecule.

CHAPTER IV

DISCUSSION

Although the results are quite reproducible for each individual junction, the results for different junctions can exhibit a variety of phenomena[78]-[80]. This is understandable as the tunneling behavior is very sensitive to many factors such as the thickness and composition of the tunneling barrier as well as the specific energy states and orientation of molecules within the junction. In our experiment, the variability of the junctions makes it difficult to predict the behavior of a single junction so that at best one can only summarize the different classes of reproducible behavior that were observed. For example in 11% of the data sets, we observed very unusual $I-V$ characteristics that were very irreproducible. These traces usually appear when the junction is freshly formed, and therefore we attribute this behavior to the mechanical instability of the freshly made junction.

In the following we are going to discuss the results from Pt+Fe/Ne/Pte, and Pt/Mn_{12}-Ac/Pt.

A. Analysis of the Dip-Peak Transition of ZBFs in Pt+Fe/Ne/Pt Junctions within the Two-Channel Kondo Model

To explain the low temperature behavior of the resistance of metals with impurities, Kondo applied the phenomenological Hamiltonian[47]

$$H_K = J\mathbf{s}\cdot\mathbf{S} + H_{reservoir} \tag{4.1}$$

to describe a magnetic impurity embedded in a host sea of electrons. In the one channel Kondo (1CK) model, the localized spin $\mathbf{S}$ of the magnetic impurity couples

antiferromagnetically with strength **J** to the spins of the electrons, **s**, in the surrounding reservoir. The properties of the free electrons in the reservoir in the absence of the magnetic impurities is described by $H_{reservoir}$.

We believe that the dip-to-peak transition observed in the Pt+Fe/Ne/Pt junctions can be modeled by a variation of the 1CK in which the localized spin can couple to two independent electron reservoirs. In the two-channel Kondo (2CK) model [81],[82], the localized spin **S** antiferromagnetically couples to two independent reservoirs of electrons [83]:

$$H_{2CK} = J_1 \mathbf{s}_1 \cdot \mathbf{S} + J_2 \mathbf{s}_2 \cdot \mathbf{S} + H_{reservoirs} \tag{4.2}$$

where $\mathbf{s}_1$ and $\mathbf{s}_2$ are spins of electrons in the surrounding two reservoir where again $H_{reservoirs}$ describes the properties of the free electrons in the reservoirs. The symmetric 2CK state is formed when the two independent channels (or reservoirs) are equally coupled to the magnetic impurity, that is, $J_1 = J_2$. Each reservoir individually attempts to screen the local spin. As they cannot both screen the spin, this causes an unstable situation resulting in a new ground state in which the local impurity is only partially screened.

Any difference in channel coupling will force the system away from the non-Fermi-liquid 2CK state and towards the 1CK state associated with the more strongly coupled reservoir. This makes the observation of the 2CK effect difficult. However, the 2Ck model has been used to describe the behavior of some heavy fermion materials [84] [85] [86]. At the 2CK symmetric point, the differential conductance should depend quadratically on the bias voltage for $eV < k_B T$ and should cross over to a $\sqrt{V}$ behavior at high bias voltages, $eV > 3k_B T$ [83]. The change in the conductance is formally given by [87]-[89]

$$\frac{\Delta G}{T^{0.5}} = \kappa Y(\frac{eV}{kT}) \tag{4.3}$$

where κ is a constant related to the Kondo temperature T_K and the scaling function $Y(x)$ is given by

$$Y(x) = \left\{ \begin{array}{cc} \frac{3}{\pi}\sqrt{x} - 1 & for \quad x \gg 1 \\ cx^2 & for \quad x \ll 1 \end{array} \right\} \tag{4.4}$$

This expression can also be rewritten as $G(V,T) = G(0,T) + BT^{1/2}\Gamma(Ax)$ when $V \gg k_BT/e$. This form was used by Agnolet et al. [64] to fit the ZBFs in their Pt/Ne/Pt tunnel junctions.

In our experiments, $x = 1$ (or equivalently $eV = k_BT$) would correspond to a bias voltage of V = 0.36 mV at a temperature of T= 4.2 K. Since the half width of the ZBFs is about 50 mV, the major part of our ZBFs belongs to the region for which $eV > k_BT$. Although the asymptotic behavior of the differential conductance in the two extremes of bias voltage: $V \approx 0$ and $V \gg k_BT/e$ is known, there is no analytical solution for the relation between the conductance and the voltage at intermediate voltages. A numerical solution for the scaling function was obtained from Dr. J. V. Delft [90] and was used to fit our data.

In Figs. 27 and 28, we show the comparisons between the scaling function and our experimental data. Fitting the data to the equation $G(V,T) = G(0,T) + BT^{1/2}\Gamma(Ax)$ again, we found that A=0.06 and $B = 0.00041\ K^{-1/2}e^2/h$, for the dip (Fig. 27), and A=0.0025 and $B = 0.0011\ K^{-1/2}e^2/h$, for the peak (Fig. 28).

The 2CK model mentioned above is not the only model that can explain the scaling property of ZBF. Wingreen, Altshuler and Meir[91] have pointed out that a model based on disorder could also generate a similar scaling function. However, J.

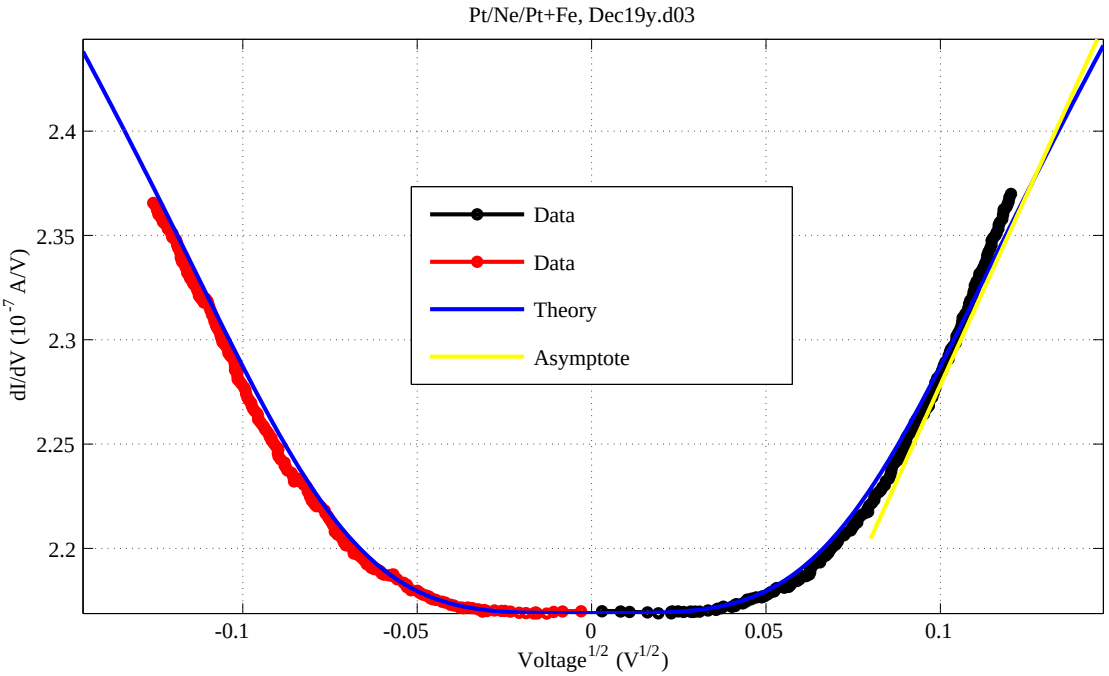

Fig. 27. Comparison between the 2CK model and the ZBF (dip) for a Pt+Fe/Ne/Pt junction. When $V^{1/2}$ is plotted on the horizontal axis, the relation between the conductance (black and red dots) and the scaling function (blue line) should be a straight line.

V. Delf et al. [92] showed that this type of model would contradict other important experimental facts. Furthermore, the agreement between the experimental and theoretical scaling curves found in reference [91] was the result of an error in the analysis [93]; once the error is corrected, the agreement ceases.

B. Analysis of the ZBFs of Pt/Mn_{12}-Ac/Pt Junctions within the Kondo Resonance Model

Although the Pt/ Mn_{12}-Ac/Pt junctions also exhibit ZBFs, unlike the Pt+Fe/Ne/Pt junctions, they are often asymmetric with respect to the bias voltage. We therefore will analyze them in terms of the Fano resonance discussed in Chapter I. Within the

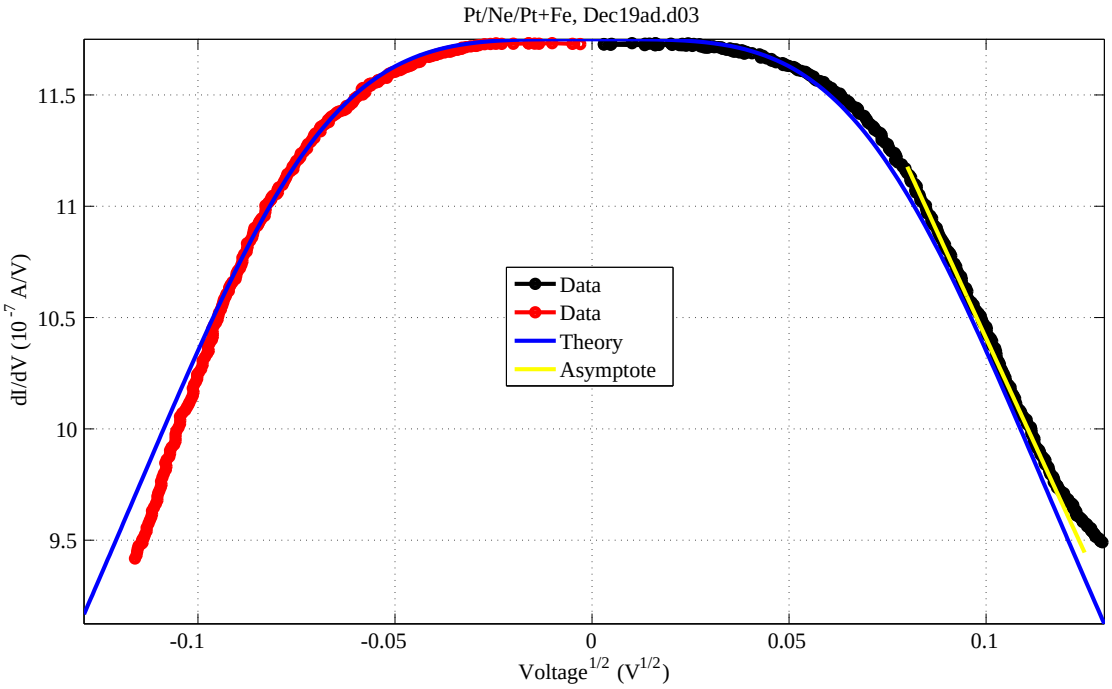

Fig. 28. Comparison between the 2CK model and the ZBF (peak) for a Pt+Fe/Ne/Pt junction. When $V^{1/2}$ is plotted on the horizontal axis, the relation between the conductance (black and red dots) and the scaling function (blue line) should be a straight line.

Anderson model[51], a Mn_{12}-Ac molecule on the surface of platinum can be thought of as a discrete orbital in resonance with the continuum of electron conduction band states. An electron tunneling from one wire to the Kondo resonance has contributions from the orbital and the continuum channels which leads to an additional quantum interference term. The differential conductance, dI/dV, of the tunnel junction, gives a measure of the rate of electronic transitions from the state at E_F (Fermi energy) on the negatively biased wire to the states at $E_F + eV$ on the positively biased wire. In another words, it is a measure of the density of electronic-like excitations of the positively biased wire that have energy eV measured with respect to E_F. Thus one can measure the spectra of the Kondo resonance by measuring dI/dV.

Based on Eq. (1.19), we used the following equation to fit the $dI/dV - V$ curves in our experiments

$$\frac{dI}{dV} = P1 + P2 \cdot \frac{[(V + P3) + P4]^2}{(V + P3)^2 + P5} \tag{4.5}$$

where

$$q = P4 \Big/ \sqrt{P5}, \;\; k_B \cdot T_K \approx \sqrt{P5}$$

One such fit is shown in Fig. 29. For this fit, we obtain $q = 0.0935$, $\alpha = 4.7$ meV, and $T_K = 613$ K. We can see that Kondo resonance gives an asymmetric curve rather than the symmetric one yielded by 2CK effect. The fit are typically poor for large bias voltages $|V| > 50$ mV. Other effects such as inelastic tunneling [9], [94] and changes due to electron trapping may need to be removed to improve the fit.

Fitting 132 sets of data [95], we obtained the average values q=1.9±10.5, α=-1.5±8.7 meV, and T_K= 290±154 K. Data sets with extreme values of the fitted parameters (T_K > 1000 K or <100 K, q<-0.5 and $|\alpha|$>50) were excluded from the average. Because the data are obtained from many different junctions, it is not a surprise to see such large deviations. Different numbers, different configurations, different positions of the Mn_{12}-Ac molecules can all result in different values of q and α. Although the variations in the values of T_K is relatively small, T_K can also depend upon the configuration of the molecules [50].

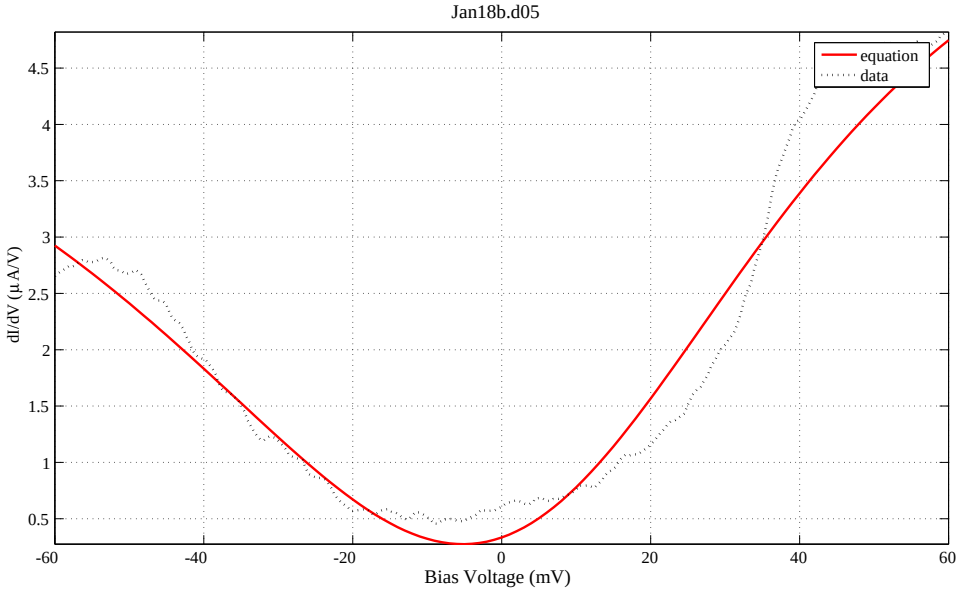

Fig. 29. dI/dV data (black) from a Pt/Mn_{12}-Ac/Pt junction with a fit to the Kondo resonance model (red) with parameter values of $P(1) = 0.2746$, $P(2) = 6.1553$, $P(3)$ = -0.0047, $P(4) = 0.0049$, $P(5) = 0.0028$ corresonding to $T_K = 613$ K, $q = 0.0935$, $\alpha = 4.7$ meV.

REFERENCES

[1] "The Atomistic Philosophy of Leucippus and Democritus", http://www.thebigview.com/greeks/democritus.html, accessed April (2008).

[2] J.J. Thomson, "Cathode Rays," Philosophical Magazine, **44**, 293 (1897).

[3] M. Planck, "On the Law of Distribution of Energy in the Normal Spectrum," Ann. Der Physik, **4**, 553 (1901).

[4] G. Gamow, "Zur Quantentheorie de Atomkernes," Z. Phys., **51**, 204 (1928).

[5] J. R. Oppenheimer, "Three Notes on the Quantum Theory of Aperiodic Effects," Phys. Rev., **31**, 66 (1928).

[6] R.H. Fowler, and L. Nordheim, "Electron Emission in Intense Electric Fields," Proc. Roy. Soc., **A119**, 173 (1928).

[7] R. Young, J. Ward, and F. Scire, "The Topografiner: An Instrument for Measuring Surface Microtopography," Rev. Sci. Instrum., **43**, 999 (1972).

[8] G. Binnig, H. Rohrer, Ch. Gerber, and E. Weibel, "7 $\times$ 7 Reconstruction on Si(111) Resolved in Real Space," Phys. Rev. Lett., **50**, 120 (1983).

[9] R.C. Jaklevic and J. Lambe, "Molecular Vibration Spectra by Electron Tunneling," Phys. Rev. Lett., **17**, 1139 (1966).

[10] D.T. Zimmerman, "Vibrational Spectroscopy of Adsorbed Molecules Using Self-Assembling Tunnel Junctions," Ph.D. dissertation. Texas A&M University, College Station, TX (1997).

[11] J. R. Kirtley and P. K. Hansma, "Effect of the Second Metal Electrode on Vibrational Spectra in Inelastic-electron-tunneling Spectroscopy," Phys. Rev. B, **12**, 531 (1975).

[12] P. K. Hansma, *In Tunneling Spectroscopy: Capabilities, Applications and New Techniques*, edited by P.K. Hansma (Plenum, New York, 1982).

[13] S. Gregory, "Inelastic Tunneling Spectrocopy and Single-Electron Tunneling in an Adjustable Microscopic Tunnel Junction," Phys. Rev. Lett., **64**, 689 (1990).

[14] S. Gregory, "Experimental Observation of Scattering of Tunneling Electrons by a Single Magnetic Moment," Phys. Rev. Lett., **68**, 2070 (1992).

[15] D.T. Zimmerman, M.B. Weimer, and G. Agnolet, "An Adjustable Oxide-free Tunnel Junction for Vibrational Spectroscopy of Molecules," Appl. Phys. Lett., **75**, 2500 (1999).

[16] D.T. Zimmerman and G. Agnolet, "Inelastic Electron Tunneling Spectroscopy Measurements Using Adjustable Oxide-free Tunnel Junctions," Rev. Sci. Instrum., **72**, 1781 (2001).

[17] R. Sessoli, D. Gatteschi, A. Caneschi, & M. A. Novak, "Magnetic Bistability in a Metal-ion Cluster," Nature, **365**, 141 (1993).

[18] R. Sessoli, H. -L. Tsai, A. R. Schake, S. Wang, J. B. Vincent, K. Folting, D. Gatteschi; G. Christou, D. N. Hendrickson, "High-spin Molecules: $[Mn_{12}O_{12}(O_2CR)_{16}(H_2O)_4]$," J. Am. Chem. Soc., **115**, 1804 (1993).

[19] E.M. Chudnovsky and J. Tejada, *Macroscopic Quantum Tunneling of the Magnetic Moment, Cambridge Studies in Magnetism*, Vol. 4 (Cambridge University Press, Cambridge, 1998).

[20] S. M. J. Aubin, M. W. Wemple, D. M. Adams, H. -L. Tsai, G. Christou, D. N. Hendrickson, "Distorted $Mn^{IV}Mn^{III}{}_3$ Cubane Complexes as Single-Molecule Magnets," J. Am. Chem. Soc., **118**, 7746 (1996).

[21] C. Joachim, J.K. Gimzewski, and A. Aviram, "Electronics Using Hybrid-Molecular and Mono-molecular Devices," Nature, (London) **408**, 541 (2000).

[22] G. Christou, D. Gatteschi, and D. N. Hendrickson,and R. Sessoli, "Single-Molecule Magnets," MRS Bulletin, **25**, 66 (2000).

[23] D. Gatteschi, and R. Sessoli, "Quantum Tunneling of Magnetization and Related Phenomena in Molecular Materials,"Angew. Chem. Int. Ed. Engl., **42**, 268 (2003).

[24] J. R. Friedman, M. P. Sarachik, J. Tejada, and R. Ziolo, "Macroscopic Measurement of Resonant Magnetization Tunneling in High-Spin Molecules," Phys. Rev. Lett., **76**, 3830 (1996).

[25] H. J. Eppley, H.-L.Tsai, N. de Vries, K. Folting, G. Christou, and D. N. Hendrickson, "High-Spin Molecules: Unusual Magnetic Susceptibility Relaxation effects in $[Mn_{12}O_{12}(O_2CEt)_{16}(H_2O_3)]$ (S=9) and the One-Electron Reduction Product $(PPh_4)[Mn_{12}O_{12}(O_2CEt)_{16}(H_2O)_4]$ (S=19/2)," J. Am. Chem. Soc., **117**, 301 (1995).

[26] J. A. A. J. Perenboom, J. S. Brooks, S. Hill, T. Hathaway, and N. S. Dalal, "Relaxation of the Magnetization of Mn_{12} Acetate," Phys. Rev. B, **58**, 330 (1998).

[27] L. Thomas, F. Lionti, R. Ballou, D. Gatteschi, R. Sessoli, and B. Barbara, "Macroscopic Quantum Tunneling of Magnetization in a Single Crystal of Nanomagnets," Nature, **383**, 145 (1996).

[28] L. Bokacheva, A. D. Kent, and M. A. Walters, "Crossover between Thermally Assisted and Pure Quantum Tunneling in Molecular Magnet Mn_{12}-Acetate," Phys. Rev. Lett., **85**, 4803 (2000).

[29] Y. Furukawa, K. Watanabe, K. Kumagai, Z. H. Jang, A. Lascialfari, F. Borsa, and D. Gatteschi, "Ground-state Magnetization of the Molecular Cluster $Mn_{12}O_{12}$-acetate as Seen by Proton NMR," Phys. Rev. B, **62**, 14246 (2000).

[30] T. Lis, "Preparation, Structure, and Magnetic Properties of a Dodeeanuelear Mixed-Valence Manganese Carboxylate," Acta Crystallogr., **B36**, 2042 (1980).

[31] D. Gatteschi, R. Sessoli and A. Cornia, "Single-molecule Magnets Based on Iron(III) Oxo Clusters," Chem. Commun., 725 (2000).

[32] D. D. Awschalom, D. P. Di Vincenzo, and J. F. Smyth, "Macroscopic Quantum Effects in Nanometer-Scale Magnets," Science, **258**, 414 (1992).

[33] J. Means, V. Meenakshi, R.V.A. Srivastava, W. Teizea, Al.A. Kolomenskii, H.A. Schuessler, H. Zhao, K.R. Dunbarb, "Films of Mn_{12}-acetate Deposited by Low-Energy Laser Ablation," J. Magnetism and Magnetic Materials, **284**, 215 (2004).

[34] V. Meenakshi, W. Teizer, D.G. Naugle, H. Zhao, K.R. Dunbar, "Films of Mn12-acetate by Pulsed Laser Evaporation," Solid State Communications, **132**, 471 (2004).

[35] D. Seo, W. Teizer, H. Zhao, K.R. Dunbar, "Enhanced Alignment of Mn_{12}-acetate Micro-crystals," J. Magnetism and Magnetic Materials, **301**, 31 (2006).

[36] M. Clemente-León, H. Soyer, E. Coronado, C. Mingotaud, C.J. Gómez-Garcia, P. Delhaés, "Langmuir-Blodgett Films of Single-Molecule Nanomagnets," Angew. Chem. Int. Ed., **37**, 2842 (1998).

[37] D. Ruiz-Molina, M. Mas-Torrent, J. Gómez, A.I. Balana, N. Domingo, J. Tejada, M.T. Martinez, C. Rovira, "Isolated Single-Molecule Magnets on the Surface of a Polymeric Thin Film," J. Veciana. Adv. Mater., **15**, 42 (2003).

[38] A. Cornia, A.C. Fabretti, M. Pacchioni, L. Zobbi, D. Bonacchi, A. Caneschi, D. Gatteschi, R. Biagi, U. Del Pennino, V. De Renzi, L. Gurevich, H.S.J. Van der Zant, "Direct Observation of Single-Molecule Magnets Organized on Gold Surfaces," Angew. Chem. Int. Ed., **42**, 1645 (2003).

[39] J.M. North, D. Zipse, and N.S. Dalal, E.S. Choi, E. Jobiliong, J.S. Brooks, and D.L. Eaton, "Semiconductive and Photoconductive Properties of the Single-molecule Magnets Mn_{12}-acetate and Fe_8Br_8," *Phys. Rev. B*, **67**, 174407 (2003).

[40] J.C. Fisher and I, Giaever, "Tunneling Through Thin Insulating Layers," J. Appl. Phys., **32**, 172 (1961).

[41] A. Sommerfeld and H. Bethe, *Handbuch der Physik von Geiger und Scheel*, Vol. 24/2, (Julius Spring - Verlag, Berlin, 1933), p. 450.

[42] R. Holm, "The Electric Tunnel Effect Across Thin Insulator Films in Contacts," J. Appl. Phys., **22**, 569 (1951).

[43] R. Holm and B. Kirschstein, "About the Resistance of the Thinnest Fremdschichten in Metal Contacts", Z. Tech, Physik, **16**, 488 (1935).

[44] J.G. Simmons, "Generalized Formula for the Electric Tunnel Effect between Similar Electrodes Separated by a Thin Insulating Film," J. Appl. Phys., **34**, 1793 (1963).

[45] B.H. Bransden & C.J. Joachain, *Quantum Mechanics*, Second edition, (Benjamin-Cummings Publishing Company, San Francisco, CA. 2000).

[46] W.F. Brinkman, R.C. Dynes, and J.M. Rowell, "Tunneling Conductance of Asymmetric Barrier," J. Appl. Phys., **41**, 1915 (1970).

[47] J. Kondo, "Resistance Minimum in Dilute Magnetic Alloys," Prog. Theor. Phys., **32**, 37 (1964).

[48] A. C. Hewson, *The Kondo Problem to Heavy Fermions*, (Cambridge Univ. Press, Cambridge, UK, 1993).

[49] G. Gruner and A. Zawadowski, "Magnetic Impurities in Non-magnetic Metals," Rep. Prog. Phys., **37**, 1497 (1974).

[50] V. Madhavan, W. Chen, T. Jamneala, M. F. Crommie, N. S. Wingreen, "Tunneling into a Single Magnetic Atom: Spectroscopic Evidence of the Kondo Resonance," Science, **280**, 567 (1998).

[51] P. W. Anderson, "Localized Magnetic States in Metals," Phys. Rev., **124**, 41 (1961).

[52] J.W. Allen, *Synchrotron Radiation Research: Advances in Surface and Interface Science*, vol. 1, edited by R.Z. Bachrach, (Plenum, New York, 1992).

[53] U. Fano, "Effects of Configuration Interaction on Intensities and Phase Shifts," Phys. Rev., **124**, 1866 (1961).

[54] Y. Meir and N. S. Wingreen, "Landauer Formula for the Current through an Interacting Electron Region," Phys. Rev. Lett., **68**, 2512 (1992).

[55] A. Houtghton, N. Read, H. Won, "1/N Expansion for the Transport Coefficients of the Single-impurity Anderson Model", Phys. Rev B, **35**, 5123 (1987).

[56] D. Lang, "Spectroscopy of Single Atoms in the Scanning Tunneling Microscope, " Phys. Rev B, **34**, 5947 (1986).

[57] Minco Products, Inc., Minneapolis, MN, Table 3-100.

[58] ICS Electronics Corp., Milpitas, CA.

[59] 2 Ampere, 0.025" in diameter. Bussmann MFG Div., Mc Graw-Edison Co., St. Louis 7, MO.

[60] G. T. Furukawa, W. G. Saba, D. M. Sweger, H. H. Plumb, "Normal Boiling Point and Triple Point Temperatures of Neon," Metrologia, **6**, Issue 1, pp. 35-37 (1970).

[61] "Metastable Neon Atoms", http://www.iqo.uni-hannover.de/ertmer/nebec/, accessed April (2008).

[62] "Chemical Properties of Platinum, Electron Work Function", http://environmentalchemistry.com/yogi/periodic/Pt.html, accessed April (2008).

[63] P. A. Tipler, and R. A. Llewellyn, *Modern Physics*, 3rd Ed., (W.H. Freeman, New York, NY, 1999).

[64] G. Agnolet, S. R. Savitski, D, T. Zimmerman, "Zero Bias Features in Self-assembling Tunnel Junctions," Physica B, **284-288**, 1840 (2000).

[65] J. von Delft, A.W.W. Ludwig, V. Ambegaokar, "The 2-Channel Kondo Model II: CFT Calculation of Non-Equilibrium Conductance through a Nanoconstriction containing 2-Channel Kondo Impurities," Ann. Phys., **273**, 175 (1999).

[66] H.B. Heersche, Z. de Groot, J.A. Folk, and H.S.J. van der Zant, C. Romeike and M.R. Wegewijs, L. Zobbi, D. Barreca, E. Tondello, and A. Cornia, "Electron Transport through Single Mn_{12} Molecular Magnets," Cond-mat/0510732, **v2**, 29 Mar 2006.

[67] M. H. Jo, J. E. Grose, K. Baheti, M. M. Deshmukh, J. J. Sokol, E. M. Rumberger, D. N. Hendrickson, J. R. Long, H. Park, and D.C. Ralph, "Signatures of Molecular Magnetism in Single-Molecule Transport Spectroscopy," Nano Lett., **6**, 2014 (2006).

[68] H. Park, J. Park, A. K. L. Lim, E. H. Anderson, A. P. Alivisatos, and P. L. McEuen, "Nanomechanical Oscillations in a Single-C60 Transistor," Nature, **407**, 57 (2000).

[69] J. Park, A. N Pasupathy, J. I. Goldsmith, C. Chang, Y. Yaish, J. R. Petta, M. Rinkoski, J. P. Sethna, H. D. Abruna, P. L. McEuen, and D. C. Ralph, "Coulomb Blockade and the Kondo Effect in Single-atom Transistors," Nature, **417**, 722 (2002).

[70] W. Liang, M. P. Shores, M. Bockrath, J. R. Long and H. Park, "Kondo Resonance in a Single-molecule Transistor," Nature, **417**, 725 (2002)

[71] J.B. Barner and S.T. Tuggiero, "Observation of the Incremental Charging of Ag Particles by Single Electrons," Phys. Rev. Lett., **59**, 807 (1987).

[72] C.W.J. Beenakker, "Theory of Coulomb-blockade Oscillations in the Conductance of a Quantum Dot," Phys. Rev. B, **44**, 1646 (1991).

[73] K. Mullen and E. Ben-Jacob, R.C. Jaklevic, and Z. Schuss, "I-V Characteristics of Coupled Ultrasmall-capacitance Normal Tunnel Junctions," Phys. Rev. B. **37**,

98 (1988).

[74] C.T. Rogers and R.A. Buhrman, "Nature of Single-localized-electron States Derived from Tunneling Measurements," Phys. Rev. Lett., **55**, 859 (1985).

[75] California Fine Wire company, Grover Beach, CA.

[76] A.N. Pasupathy, "Electron Transport in Molecular Transports," Ph.D. thesis, Cornell University, Ithaca, NY. (2004).

[77] A. N. Pasupathy, J. Park, C. Chang, A. V. Soldatov, S. Lebedkin, R. C. Bialczak, J. E. Grose, L. A. K. Donev, J. P. Sethna, D. C. Ralph, P. L. McEuen, "Vibration-assisted Electron Tunneling in C140 Single-molecule Transistors," Nano Lett., **5**, 203 (2005).

[78] L. H. Yu, Z. K. Keane, J.W. Ciszek, L. Cheng, M. P. Stewart, J. M. Tour, and D. Natelson, "Inelastic Electron Tunneling via Molecular Vibrations in Single-Molecule Transistors," Phys. Rev. Lett., **93**, 26802 (2004).

[79] L. H. Yu and D. Natelson, "Zero-bias Anomalies in Electrochemically Fabricated Nanojunctions," Appl. Phys. Lett., **82**, 2332 (2003).

[80] L. H. Yu, Z. K. Keane, J.W. Ciszek, L. Cheng, J. M. Tour, T. Baruah, M. R. Pederson, and D. Natelson, "Kondo Resonances and Anomalous Gate Dependence in the Electrical Conductivity of Single-Molecule Transistors," Phys. Rev. Lett., **95**, 256803 (2005).

[81] P. Nozieres, & A. Blandi, "Kondo Effect in Real Metals," J. Phys., **41**, 193 (1980).

[82] A. Zawadowski, "Kondo-like State in a Simple Model for Metallic Glasses," Phys. Rev. Lett., **45**, 211 (1980).

[83] R.M. Potok, I.G. Rau, H. Shtrikman, Y. Oreg & D. Goldhaber-Gordon, "Observation of the Two-channel Kondo Effect," Nature, **446**, 167 (2007).

[84] D.L. Cox, "Quadrupolar Kondo Effect in Uranium Heavy-electron Materials," Phys. Rev. Lett., **59**, 1240 (1987).

[85] C.L. Seaman, M.B. Maple, B.W. Lee, and S. Ghamaty, M.S. Torikachivili, J.-S. Kang, L.Z. Liu, and J.W. Allen, D.L. Cox. "Evidence for Non-Fermi-liquid Behavior in the Kondo Alloy $Y_{1-x}U_xPb_3$," Phys. Rev. Lett., **67**, 2882 (1991).

[86] M. J. Besnus, M. Benakki, A. Braghta, H. Danan, G. Fischer, J. P. Kappler, A. Meyer and P. Panissod, "Specific-heat and NMR of the Kondo System $YbPD_2Si_2$," J. Magn. Magn. Mater., **76-7**, 471 (1988).

[87] I. Affleck, & A.W.W. Ludwig, "Exact Conformal-field-theory Results on the Multichannel Kondo Effect: Single-fermion Green's Function, Self-energy, and Resistivity," Phys. Rev. B, **48**, 7297 (1993).

[88] D.C. Ralph, A.W.W. Ludwig, J. von Delft, & R.A. Buhrman, "2-channel Kondo Scaling in Conductance Signals from 2-level Tunneling Systems," Phys. Rev. Lett., **72**, 1064 (1994).

[89] M.H. Hettler, J. Kroha, & S. Hershfield, "Nonlinear Conductance for the Two Channel Anderson Model," Phys. Rev. Lett., **73**, 1967 (1994).

[90] Private communication with Dr. J. von Delft at Universität Karlsruhe, Germany.

[91] N. S. Wingreen, B. L. Altshuler and Y. Meir, "Comment on '2-Channel Kondo Scaling in Conductance Signals from 2-Level Tunnel Systems,' " Phys. Rev. Lett., **75**, 769 (1995).

[92] J. von Delft and D. C. Ralph, R. A. Buhrman, S. K. Upadhyay and R. N. Louie, A. W. W. Ludwig, and V. Ambegaokar "The 2-Channel Kondo Model I. Review of Experimental Evidence for Its Realization in Metal Nanoconstrictions," Ann. Phys., **263**, 1 (1998).

[93] N. S. Wingreen, B. L. Altshuler, and Y. Meir, "Erratum: Comment on '2-Channel Kondo Scaling in Conductance Signals from 2-Level Tunneling Systems'," Phys. Rev. Lett., **81**, 4280 (1998).

[94] D.T. Zimmerman, M.B. Weimer, and G. Agnolet, "An Adjustable Oxide-free Tunnel Junction for Vibrational Spectroscopy of Molecules," Appl. Phys. Lett., **75**, 2500 (1999).

[95] One dewar of LHe can last $\sim$ 15 days. One Pt+Mn_{12}-Acetate wire is mainly used and the other one is as a backup. Once the junction is formed, we will take data until we believe we have obtained all of the necessary data. Then we will break the junction and then form a new junction. New characters usually appear even though the junction is formed between the same two wires since the junction is not necessarily formed at the exactly same spot. We do use the backup wire when either there is no new phenomenon can be observed or the main wire simply can't form a junction.

APPENDIX A

APPROXIMATION OF INTEGRATION

One can integrate an arbitrary function $f^{1/2}$,

$$\int_{s1}^{s2} f^{\frac{1}{2}}(x)dx, \tag{A.1}$$

in terms of the average of the function $\overline{f}$ defined as

$$\overline{f} = \frac{1}{\Delta s}\int_{s1}^{s2} f(x)dx \tag{A.2}$$

where $\Delta s = s_2 - s_1$. Equation (A.1) is first written as

$$\int_{s1}^{s2} f^{\frac{1}{2}}(x)dx = \overline{f^{\frac{1}{2}}}\int_{s1}^{s2}\left\{1 + \frac{f(x)-\overline{f}}{\overline{f}}\right\}^{\frac{1}{2}} dx \tag{A.3}$$

Expanding Eq. (A.3) and neglecting terms in $[(f(x)-\overline{f})/\overline{f}]^3$ and higher powers,

$$\int_{s1}^{s2} f^{\frac{1}{2}}(x)dx = \overline{f^{\frac{1}{2}}}\int_{s1}^{s2}\left\{1 + \frac{f(x)-\overline{f}}{2\overline{f}} - \frac{[f(x)-\overline{f}]^2}{8\overline{f}^2}\right\} dx. \tag{A.4}$$

The integral of the second term in the brackets is zero [as defined by Eq. (A.2)]; thus, Eq. (A.4) integrates to

$$\begin{aligned}\textstyle\int_{s1}^{s2} f^{\frac{1}{2}}(x)dx &\approx \overline{f^{\frac{1}{2}}}\Delta s\left\{1 - \tfrac{1}{8\overline{f}^2\Delta s}\textstyle\int_{s1}^{s2}[f(x)-\overline{f}]^2dx\right\} \\ &= \beta\overline{f^{\frac{1}{2}}}\Delta s,\end{aligned} \tag{A.5}$$

where

$$\beta = 1 - \frac{1}{8\overline{f}^2 \Delta s} \int_{s1}^{s2} [f(x) - \overline{f}]^2 dx \tag{A.6}$$

Usually

$$1 \gg \frac{1}{8\overline{f}^2 \Delta s} \int_{s1}^{s2} [f(x) - \overline{f}]^2 dx$$

that is $\beta \approx 1$. Thus,

$$\int_{s1}^{s2} f^{\frac{1}{2}}(x) dx = \overline{f^{\frac{1}{2}}} \Delta s. \tag{A.7}$$

VITA

Lianxi Ma received his B.S. and M.S. in physics from Hebei University in China in 1983 and 1993 respectively. He obtained his Ph.D. degree in plasma physics from the Institute of Physics, Chinese Academy of Sciences in 1996. He worked as an associate professor of physics in China University of Geosciences, Beijing, before coming to Texas A&M University in 1999. His address is:

Department of Physics
c/o Dr. Glenn Agnolet
Texas A&M University M.S. 4242
College Station, TX 77843.

His email address is: malianxi@gmail.com.